Heterogeneities in stress and strength in Tohoku and its relationship with earthquake sequences triggered by the 2011 M9 Tohoku-Oki earthquake

Keisuke Yoshida[1], Akira Hasegawa[1], Takeyoshi Yoshida[2], Toru Matsuzawa[1]

1: Research Center for Prediction of Earthquakes and Volcanic Eruptions, Graduate School of Science, Tohoku University

2: Institute of Mineralogy, Petrology, and Economic Geology, Graduate School of Science, Tohoku University

Corresponding author: Keisuke Yoshida, Research Center for Prediction of Earthquakes and Volcanic Eruptions, Tohoku University, 6-6 Aza-Aoba, Aramaki, Aoba-ku, Sendai, 980-8578, Japan. (keisuke.yoshida.d7@tohoku.ac.jp)

Abstract

Inland Tohoku has been recognized as being under the WNW-ESE compressional stress state before the 2011 M9 Tohoku-Oki earthquake. Earthquakes that occurred there were characterized by reverse faulting with compressional axis oriented almost WNW-ESE direction. The Tohoku-Oki earthquake reduced this WNW-ESE compressional stress and, therefore, should have suppressed the earthquake occurrence. However, several intensive earthquake sequences were triggered in inland Tohoku. In this study, we investigated the triggering mechanism of these remote earthquake sequences in the stress shadow based on the detailed distribution of stress orientations newly determined from pre-mainshock focal mechanism data. The spatial distribution of stress orientations shows that there exist some regions with anomalous stress fields even before the Tohoku-Oki earthquake on the spatial scale of a few tens of kilometers. This spatial heterogeneity in stress field suggests that the differential stress magnitude in inland Tohoku is low (a few tens of MPa). Locations of the earthquake clusters tend to correspond to regions where the principal stress axis orientations of the pre-mainshock period are similar to those of the static stress change by the Tohoku-Oki earthquake. This observation suggests that these earthquake sequences were triggered by local increase in differential stress due to the static stress change. However, a few swarm sequences occurred in central Tohoku with delays ranging

from a few days to few weeks after the Tohoku-Oki earthquake despite the reduction in differential stress. These sequences have notable characteristics including upward migration of hypocenters. Such features are similar to the fluid-injection induced seismicity. The source regions of these swarms are located near the ancient caldera structures and geological boundaries. The swarm activities were probably triggered by the upward fluid movement along such pre-existing structures. These observations demonstrate that information about the temporal evolutions of both stress and frictional strength is necessary to understand the triggering mechanism of earthquakes.

1. Introduction

To obtain a comprehensive view of the earthquake generation process, it is necessary to understand the triggering mechanism of aftershocks or induced earthquakes after a large earthquake. In general, an earthquake occurs when the shear stress acting on a plane exceeds the frictional strength of the plane. We can use the Coulomb failure criterion as a simple approximation of the condition of the earthquake occurrence:

$$\tau = \mu(\sigma_{\mathrm{n}} - P_{\mathrm{P}}) \tag{1}$$

where τ is shear stress, μ is coefficient of friction, σ_{n} is normal stress, and P_{P} is pore pressure. Based on this equation, we can consider two causes for the occurrence of an earthquake: increases in shear stress τ and decreases in frictional strength $\mu(\sigma_{\mathrm{n}} - \sigma_{\mathrm{P}})$ (e.g., Hainzl & Fischer, 2002). It has been suggested that both, accumulation of stress and reduction in frictional strength due to elevated pore pressure play an important role in earthquake generation (e.g., Hasegawa, 2017; Hubbert & Rubey, 1959; Miller, 2013; Nur & Booker, 1972; Rice, 1992; Sibson, 1992). Thus, the knowledge of the temporal change in stress and pore pressure after a large earthquake is essential to understand the triggering of an earthquake. In particular, the following effects can be considered: coseismic Coulomb's stress increase by static deformation and dynamic wave propagation, postseismic Coulomb's stress increase by postseismic slip and viscoelastic response,

elastic interaction among triggered earthquakes, and the effect of pore pressure change associated with these processes.

The 2011 M9 Tohoku-Oki earthquake caused numerous earthquakes along the plate boundary, within the overriding plate, and within the subducting slab (Asano et al., 2011; Ishibe et al., 2011; Toda et al., 2011; Yukutake et al., 2011; Miyazawa et al., 2011; Okada et al., 2011; Lengliné et al., 2012; Enescu et al., 2012; Kato et al., 2013; Yukutake et al., 2013; Shimojo et al., 2014). A number of earthquakes took place in inland Japan (Fig. 1), which is densely covered by the nationwide seismic network. This provides a unique opportunity to study the mechanism of remote earthquake triggering.

The focal mechanisms of these earthquakes triggered by the Tohoku-Oki earthquake are readily explained by the static stress change by the Tohoku-Oki mainshock (e.g., Asano et al., 2011; Chiba et al., 2013; Hasegawa et al., 2011; Hasegawa et al., 2012; Hasegawa & Yoshida, 2015; Nakajima et al., 2013; Yoshida et al., 2012). (1) Interplate aftershocks do not occur inside the large slip area of the mainshock rupture. They instead focus on the edge of the large slip area (Asano et al., 2011; Hasegawa et al., 2012; Kato and Igarashi, 2012; Nakamura et al., 2016). This feature can be well explained by the redistribution of shear stress inside and around the mainshock slip region. (2) Aftershocks within the subducting Pacific plate intensely occurred in the eastern and the western

extensions of the large slip region of the mainshock rupture. P-axes of earthquake focal mechanisms were oriented to WNW-ESE in the western extension parallel to the coseismic slip direction, while T-axes were oriented to this direction in the eastern extension (Chiba et al., 2013; Hasegawa & Yoshida, 2015). This pattern is also well explained by the effect of the static stress change caused by the mainshock slip. (3) Numerous normal fault earthquakes occurred in the overriding plate above the source region of the mainshock (Asano et al., 2011; Hasegawa et al., 2012). Such normal fault earthquakes were scarcely observed before the Tohoku-Oki mainshock, which suggests that the stress field rotated after the Tohoku-Oki earthquake by its static stress change (Hasegawa et al., 2011, 2012; Hardebeck, 2012). These normal fault earthquakes seem to almost continuously occur from just above the large slip region to the Fukushima-Ibaraki border region near the Pacific coast. (4) In the Chubu-Kanto district in inland Japan, seismicity rate increased. In this region, the background stress field was characterized by NW-SE compression similar to the static stress change by the mainshock rupture. Yoshida et al. (2012) suggested that the increase in seismicity rate was caused by the increase in differential stress. (5) Even in regions very far from the source region of the Tohoku-Oki mainshock (the static stress change < 0.001 MPa), some earthquake sequences were triggered probably due to the dynamic wave propagation and the associated pore pressure

change (Enescu et al., 2012; Kato et al., 2013; Yukutake et al., 2013).

In general, the occurrence of an earthquake does not only increase the Coulomb's stress but also reduces it depending on location, referred to as the stress shadow (e.g., Simpson & Reasenberg, 1994), even on fault planes with the same specific orientation by the modulation of stress field. Inland Tohoku was recognized as being under the WNW-ESE compressional reverse faulting stress regime before the Tohoku-Oki earthquake (e.g., Hasegawa et al., 1994; Terakawa and Matsu'ura, 2010; Townend and Zoback, 2006; Yoshida et al., 2012). Indeed, all of recent large (M>6) earthquakes have reverse faulting focal mechanisms with P-axis oriented to WNW-ESE. This WNW-ESE compressional stress was at least partly formed by the mechanical coupling along the plate boundary (e.g., Suwa et al., 2006). The Tohoku-Oki earthquake reduced this WNW-ESE compressional stress and, therefore, the differential stress (Fig. 1), producing a stress shadow, especially in inland Tohoku, with the typical NNE-SSW striking reverse fault. Therefore, it should have suppressed the earthquake occurrence in inland Tohoku. However, intensive earthquake sequences were activated in inland Tohoku after the Tohoku-Oki event. Thus, the triggering mechanism of earthquake sequences in inland Tohoku is not simple.

In this study, we attempt to improve our understanding of the triggering mechanism

of earthquakes in the stress shadow by focusing on the Tohoku-Oki earthquake. In the subsequent section, we review distinctive characteristics of the earthquake sequences triggered by the Tohoku-Oki earthquake in inland Tohoku, such as anomalous focal mechanisms (Section 2). We then examine the spatial distribution of the stress orientations in Tohoku to understand why earthquake sequences were triggered in inland Tohoku with anomalous focal mechanisms (Section 3). We also discuss the effect of pore pressure change, which probably played an important role in triggering the earthquake in Tohoku (Section 4).

2. Reviews of notable features of inland earthquake sequences triggered by the Tohoku-Oki earthquake

2.1 Hypocenter distribution and geological structure

Substantial earthquakes occurred in inland Tohoku just after the 2011 Tohoku-Oki earthquake. Hypocenter distributions of earthquakes in inland Tohoku for the period from March 11, 2011 to the end of 2012 are shown in Fig. 2(a). Hypocenters of events after the Tohoku-Oki earthquake are concentrated at several locations in clusters, rather than being distributed homogeneously throughout the Tohoku region. Hypocenters of earthquakes

before the Tohoku-Oki earthquake are plotted over those after the Tohoku-Oki earthquake for comparison and are shown in Fig. 2 (b). The figure indicates that intense earthquake clusters after the Tohoku-Oki earthquake were mainly located in regions where the pre-mainshock seismicity rate was quite low. This is unlike the cases of the 1992 Landers earthquake and the 1995 Hyogo earthquake, in which post-mainshock seismicity increased in proportion to the level of prior seismicity (Mallman & Zoback, 2007). Figure 2 (c) shows the earthquake occurrence time plotted against latitude. Those locations of concentrated seismicity are northern Akita (N1), southern Akita (N2), the Yamagata-Fukushima border (C1), Sendai-Okura (C2), Yamagata (C3), the Fukushima-Ibaraki border (S1), and the Tochigi-Gunma border (S2). Although hypocenters seem scattered, the earthquake occurrence rate increases in Iwate-Prefecture (N3). The geological boundaries in Tohoku are shown in Fig. 2 (b) by broken curves. The geologic boundaries go along the Fukushima-Ibaraki border (S1), Yamagata-Fukushima border (C1), Yamagata (C3), northern Akita (N1) and southern Akita (S1) earthquake clusters. All of the earthquake clusters in the central part of Tohoku (C1~C3) are located near ancient calderas (e.g., Yoshida et al., 2017).

Temporal distributions of the number of earthquakes for the period of 75 days before to 75 days after the Tohoku-Oki earthquake are shown in Fig. 3 for the eight

earthquake clusters. The required magnitude was set to 2.0. Although the completeness magnitude was relatively low just after the Tohoku-Oki earthquake (e.g., Kato et al., 2013; Yoshida et al., 2018a), the earthquake numbers still increased abruptly after the Tohoku-Oki earthquake for all these clusters. Seismicity rates were very low before the Tohoku-Oki earthquake in the focal region of these earthquake clusters. However, it was reported that the seismicity rate decreased in the aftershock area of the 2008 M7.2 Iwate-Miyagi Nairiku earthquake, which is located in central Tohoku, in the stress shadow of the Tohoku-Oki earthquake (Suzuki et al., 2013). The initiations of triggered seismic activity of the three clusters C1~C3 in central Tohoku were delayed by a few days to a few weeks after the Tohoku-Oki earthquake, while triggered seismicity of the earthquake clusters N1-N3 and S1-S2 in the northern and southern parts of Tohoku began immediately after the Tohoku-Oki earthquake (Fig. 3).

2.2 Change in focal mechanism

A notable feature of the earthquake sequences triggered by the Tohoku-Oki earthquake is significant changes in predominant focal mechanisms after the mainshock; earthquakes with anomalous focal mechanisms, such as normal faulting with the T-axes

oriented to WNW-ESE and strike-slip faulting with P-axes oriented to NNE-SSW, started to occur in a wide range of Tohoku from the region beneath the Pacific Ocean in the large slip area of the mainshock rupture (Asano et al., 2011; Hasegawa et al., 2012) to inland Tohoku apart from the source area (Kato et al., 2011; Yoshida et al., 2012). Figure 4 shows focal mechanisms of earthquakes in the overriding plate taken from Yoshida et al. (2012) and Hasegawa et al. (2012). The color shows faulting type based on the classification by Frohlich (1992). The typical focal mechanism in inland Tohoku was known to be reverse-faulting with WNW-ESE P-axis (e.g., Terakawa et al., 2010). The spatially homogeneous WNW-ESE compressional reverse fault stress regime in Tohoku was supported by geodetically measured principal strain rate axes (e.g., Kato et al, 1998; Miura et al., 2002; Sagiya et al., 2000), geological structures (e.g., Nakamura and Uyeda, 1980), earthquake focal mechanisms, and stress tensor inversion analyses (e.g., Hasegawa et al., 1994; Terakawa and Matsu'ura, 2010; Townend and Zoback, 2006; Yoshida et al., 2012). On the other hand, the earthquake clusters that occurred after the Tohoku-Oki earthquake in northern Tohoku (N1, N2) and those in southern Tohoku (S1) are characterized by strike-slip fault with NNE-SSW P-axes and normal fault with E-W~NW-SE T-axes, respectively. These focal mechanisms cannot be explained by the spatially homogeneous WNW-ESE compressional stress state which was thought to be dominant before the Tohoku-Oki

earthquake.

Three different hypotheses are suggested to explain these anomalous focal mechanisms. We summarize these hypotheses in this section as follows: a possibility of the rotation of the principal stress axes due to the static stress change of the Tohoku-Oki earthquake (Subsection 2.2.1), a possibility of the apparent stress rotation due to the pore pressure change (Subsection 2.2.2), and a possibility of the apparent stress rotation due to the stress heterogeneity in space (Subsection 2.2.3).

2.2.1 Possibility of stress rotation due to static stress change of the Tohoku-Oki earthquake

A stress tensor inversion analysis based on earthquake focal mechanisms clearly shows that the principal stress axes in the hanging-wall right above the large slip area of the mainshock rupture was rotated by the Tohoku-Oki earthquake (Hasegawa et al., 2012). Moreover, Yoshida et al., (2012) suggested that the stress axes in a couple of areas in southern Tohoku (S1) and northern Tohoku (N1, N2) also rotated after the Tohoku-Oki earthquake. The stress orientations estimated from the stress tensor inversions in inland Tohoku (Yoshida et al., 2012) along with those in the source region beneath the Pacific Ocean (Hasegawa et al., 2012) are shown in Fig. 5. The figure shows that the orientations

of the principal stress axes are significantly different before and after the Tohoku-Oki earthquake not only in the source region just above the large slip area but also in inland Tohoku. Figure 5 (c) shows the distribution of principal stress axis orientations of the static stress change of the 2011 Tohoku-Oki earthquake computed by Yoshida et al. (2012) and Hasegawa et al. (2012).

Both in the source region beneath the Pacific Ocean and in inland Tohoku, the stress orientations after the Tohoku-Oki earthquake (Fig. 5b) were similar to those of the static stress change (Fig. 5c). This suggests that the stress axes were rotated by the static stress change of the Tohoku-Oki earthquake even in inland Tohoku. If this is the case, since the stress field after the earthquake (Fig. 5b) is considered as the sum of the background stress field (Fig. 5a) and the static stress change (Fig. 5c), magnitudes of deviatoric stress tensor components before the Tohoku-Oki earthquake were smaller than that of the static stress change (Yoshida et al., 2012). Yoshida et al. (2012) quantitatively evaluated deviatoric stress magnitude before the Tohoku-Oki earthquake based on the observed stress rotation by using Wesson & Boyd's (2007) method, and concluded that the differential stress magnitude, as a representative measure of the magnitudes of deviatoric stress tensor components, before the Tohoku-Oki earthquake needs to be less than ~1 MPa in northern and southern Tohoku. Differential stress of ~1 MPa seems to contradict typically

estimated values of stress drop ranging from 1 ~ 10 MPa (e.g., Allmann & Shearer, 2009; Oth et al., 2013). We also consider other possibilities which might explain these anomalous post-earthquake focal mechanisms similar to the static stress change.

2.2.2 Possibility of apparent stress rotation due to increase in pore pressure

Increasing pore pressure can allow unfavorably-oriented fault planes, on which Coulomb's stress caused by the regional stress field are small, to slip (e.g., Sibson, 1990). A recent fluid injection test confirms that earthquakes occur even on severely mis-oriented planes in proximity to the injection well during periods of high injection rates (Martinez-Garzon et al, 2016a). If such unfavorably-oriented fault planes would be selectively activated by the increase in pore pressure, stress tensor inversion result would be biased. This could lead to apparent stress rotation after the earthquake. By considering the increase in pore pressure after the Tohoku-Oki earthquake, Terakawa et al. (2013) attempted to explain the change in focal mechanisms after the earthquake. They demonstrated that focal mechanisms in northern Akita (N1) can be explained by the regional WNW-ESE compressional stress states. However, another mechanism is necessary to explain the anomalous focal mechanisms in southern Akita (N2) and

southern Tohoku (S1) because their slip directions are largely different from those expected from the regional WNW-ESE compressional stress state. The increase in pore pressure alone does not explain why those anomalous focal mechanisms are similar to the static stress change.

2.2.3 Possibility of apparent stress rotation due to heterogeneous stress field in the considered volume

Another possibility which might explain the anomalous focal mechanisms is the effect of the spatial heterogeneity of stress orientations (e.g., Smith and Dieterich, 2010). As an example of the 1992 Landers earthquake, Hardebeck and Hauksson (2001) suggested that the stress fields rotated after the earthquake, while Townend and Zoback (2001) found the spatial heterogeneity in the stress field in and around the source region and the stress orientations remained almost stationary in the same locations.

Since the stress tensor inversion method needs to use multiple diverse focal mechanism data to constrain the stress orientation, it assumes the uniform stress orientation in a volume in which focal mechanism data are taken. Violation of this assumption can lead to an apparent rotation of stress field when combined with sample bias effects due to the static stress triggering. Figure 6 illustrates a simple situation in

which the considered volume includes subregions where the stress orientations largely differ from those in the other regions (Fig. 6a). Given that the orientation of the static stress change is similar to those in such subregions (Fig. 6b), the differential stress and thus the shear stress on optimally-oriented fault locally increases there (Fig. 6c). Earthquakes can be selectively triggered in such subregions with locally anomalous stress axes. This might lead to the observation of the apparent change in focal mechanisms, and therefore an apparent stress rotation. The spatial extent of the activation depends on the scale of the spatial change.

The spatial heterogeneity in stress orientations in inland Tohoku has been recently found by determining many focal mechanisms using data from the dense seismic network covering this area (Yoshida et al., 2015a). Yoshida et al. (2015a) found that there were regions with stress orientations largely different from the regional WNW-ESE compressional stress state. Fukushima-Ibaraki (S1) is one such region; normal fault stress regime here exists in the shallower part ($z < 12$ km) even before the Tohoku-Oki earthquake, while a reverse fault stress regime exists in the deeper portion. This should have caused the local increase in differential stress in the shallower part of the S1 region by the Tohoku-Oki earthquake because the stress orientation there is similar to the static stress change of the Tohoku-Oki mainshock. The normal fault stress regime in the

Fukushima-Ibaraki region was also found previously by Imanishi et al. (2013) who focused their stress inversion study on the earthquake sequence in this region. These observations indicate that the stress rotation in this region after the Tohoku-Oki earthquake were artefact and came from the spatial change in stress fields inside the region in which stress field is assumed to be uniform.

In northern Tohoku, the WNW-ESE compressional stress state seems to be homogeneously distributed (Fig. 5a). This WNW-ESE compressional stress and therefore differential stress should have been reduced by the Tohoku-Oki earthquake. The reason why earthquakes with such focal mechanisms, unlikely to occur under the WNW-ESE compressional stress regime, were intensively triggered in northern Tohoku after the Tohoku-Oki earthquake has not been clarified.

2.3 Summary of earthquake sequences triggered by the Tohoku-Oki earthquake in inland Tohoku

(1) The Tohoku-Oki earthquake triggered intensive earthquake sequences even in the stress shadow of inland Tohoku. Hypocenters of these triggered earthquakes were scattered in a wide area concentrated at several locations in clusters rather than being distributed homogeneously in space throughout the inland region of Tohoku (Fig. 2).

(2) Earthquakes in a few such earthquake clusters (N1, N2, S1) have strikingly different focal mechanisms, such as normal faulting type with T-axes oriented to WNW-ESE and strike-slip faulting type with P-axes oriented to NNE-SSW, from the typical one in inland Tohoku. Focal mechanisms in the two clusters N2 and S1 cannot be explained by the regional WNW-ESE compressional stress even if pore pressure increases and unfavorably-oriented fault planes selectively slip.

(3) The orientations of the stress axes which caused earthquake clusters with anomalous focal mechanisms are strikingly similar to those of the static stress change by the Tohoku-Oki earthquake. This observation suggests the two possibilities: (1) the stress axes in areas of those clusters locally rotated by the Tohoku-Oki earthquake and (2) the stress axes orientations before the Tohoku-Oki earthquake have some variations in space. The stress fields have a strong depth variation in the Fukushima-Ibaraki region (S1) and the occurrence of earthquake sequence there with many normal fault earthquakes was due to the local increases in differential stress by the static stress change of the Tohoku-Oki earthquake. In northern Tohoku, the WNW-ESE compressional stress field similar to the regional stress state is homogeneously distributed before the Tohoku-Oki earthquake. The reason why the earthquake clusters with anomalous focal mechanisms unlikely to occur under the WNW-ESE compressional stress regime are intensively activated in northern

Tohoku has not been clarified.

3. Spatial heterogeneity of stress axes in Tohoku before the Tohoku-Oki earthquake

Information about the spatial heterogeneity of the stress orientation is crucial for understanding the triggering mechanism of earthquakes as described in the previous section. In this section, we focus on inland Tohoku and examine in detail the spatial variation of the principal stress axes before the Tohoku-Oki earthquake based on new focal mechanism dataset to understand why earthquake sequences with anomalous focal mechanisms were triggered in Tohoku.

3.1 Focal mechanism data

Stress orientations are estimated by inverting focal mechanism data using the method of Michael (1987) and Hardebeck and Michael (2005). (1) We use focal new mechanism data of earthquakes for the period 1977 to 2003, which we determined in the present study. (2) Focal mechanism data determined by Yoshida et al. (2015a) for the period 1997 to the occurrence of the 2011 Tohoku-Oki earthquake are used. For the determination of focal mechanisms, we used P-wave first motion polarity data manually picked during routine processing at the Tohoku University seismic network. Focal

mechanisms were determined in the same way as Yoshida et al. (2015a) by applying the method of Hardebeck and Shearer (2002) to the P-wave polarity data. We determined focal mechanisms if the P-wave polarity data was larger than 10 and the azimuthal gap was less than 45°. In the method of Hardebeck and Shearer (2002), focal mechanism solutions are evaluated and classified into A - F ranks depending on confidence levels. Only the events with rank A or B were used here. As a result, we could determine 919 focal mechanisms. The number of focal mechanisms with rank A and B are 180 and 739, respectively. The mean numbers of polarity data used for the determination of rank A and B focal mechanisms are 38.7 and 22.7, respectively. The mean RMS values of angular differences of possible nodal planes are 18.7° and 27.5 for rank A and B focal mechanisms, respectively. Examples of focal mechanisms are shown in Fig. S1. Thus, our dataset contains a total of 3,118 focal mechanisms. The lateral distribution of focal mechanisms is shown in Fig. 7.

3.2 Stress tensor inversions

For estimating the stress orientation, we assumed that: (1) earthquakes occurred along pre-existing weak planes having various strikes and dips, (2) slip occurred in the direction of maximum resolved shear stress on those planes, and (3) the stress orientation

was uniform in the volume from which the data were taken. By the stress tensor inversion, the orientations of the principal stress axes and stress ratio $R = (\sigma 1 - \sigma 2)/(\sigma 1 - \sigma 3)$ are constrained, although their magnitudes cannot be known.

To investigate the lateral variation of the stress orientations, the study area was divided into several subareas. For each subarea, focal mechanisms were inverted assuming a homogeneous stress orientation. However, given that these results may vary depending on how the subareas are defined, we used two different approaches for subdividing the study area following Yoshida et al. (2015a, 2016a).

The first approach is similar to that of Hardebeck and Hauksson (2001). First, we placed a 5-km spaced grid net over the study area. Then, we carried out the stress inversion of Michael (1984, 1987) at each grid node using all events located within 20 km if the number of such events was <15. Otherwise, we used the 15 events closest to the grid node. If there were <10 qualifying events, we did not estimate the principal stress orientations at that grid node. In this approach, the spatial resolution of stress fields depends on the density of focal mechanisms and thus on the location. The orientations of $\sigma HMAX$ computed based on the equation by Lund and Townend (2007) are shown in Fig. 8 (a).

The second approach applies the damped stress inversion method of Hardebeck and

Michael (2006) to the focal mechanism data. This involved placing a grid with 0.5° spacing over the study area and assigning each focal mechanism to the nearest grid node. This method avoids the creation of apparent spatial variability, which is actually an artifact due to over-fitting noisy data or non- uniquely fitting data that does not completely constrain the stress tensor. The spatial damping parameter chosen was 0.6 on the basis of a trade-off between model length and data variance. The result of the stress tensor inversions is shown in Fig. 8 (b). We consider that the second approach yields a more macroscopic and stable view of stress fields than the first approach, while the first approach can provide the higher spatial resolution.

3.3 Spatial distribution of stress orientations before the Tohoku-Oki earthquake and static stress change

Figs. 8 (a) and (b) show that the stress analyses performed using the two different approaches basically yield similar results. The inland stress field is characterized by WNW-ESE compression except for the north and south outer arcs in which $\sigma 1$ axes are oriented nearly N-S and vertical, respectively. The earthquake sequences N3 and S1 are included in these north and south outer arc regions. Stress orientations are similar to the regional WNW-ESE compressional stress state in regions corresponding to the

earthquake sequences N1, N2, C1, C2, and C3 from the result of the second approach (Fig. 8b) which focuses on a macroscopic view (~ 50 km) of stress fields. On the other hand, we can see some deviations of the stress orientations in regions corresponding to the earthquake sequences N1 and N2 in the first approach (Fig. 8a) which focuses on a spatially high-resolution view of the stress field. The orientations of principal stress axes in N1 and N2 are NE-SW, which are similar to those observed after the 2011 Tohoku-Oki earthquake (Fig. 5b). This suggests that anomalous stress fields existed there even before the Tohoku-Oki earthquake and that the differential stress magnitude in inland Tohoku can be much higher than 1 MPa as estimated by Yoshida et al. (2012) based on the stress rotation after the earthquake. The difference between the first and second approaches suggests that the stress field is heterogeneous in Tohoku with a scale less than a few tens kilometers.

We estimated the static stress change of the Tohoku-Oki earthquake for comparison with the stress field before the earthquake. We used the coseismic slip distribution determined by Iinuma et al. (2012) by assuming the rigidity of 30 GPa and the Poisson's ratio of 0.25. We used the DC3D code (http://www.bosai.go.jp/study/application/dc3d/DC3Dhtml_E.html) based on the analytical solution for the homogeneous half space summarized by Okada (1992).

Although there are various published coseismic slip models (Brown et al., 2015), the results in inland Tohoku, relatively far from the source region, scarcely depend on the difference of the models (Yoshida et al., 2012; 2018a).

Spatial distribution of $\sigma 1$ and $\sigma 3$ axes of the static stress change is shown in Fig. 8 (c). The orientation of $\sigma 1$ axis is NE-SW in northern Tohoku (N1, N2), which is similar to that of the observed one before the Tohoku-Oki earthquake in the fine scale (Fig. 8a), indicating that the Tohoku-Oki earthquake lead to the local increases in differential stress. We estimated the increase or decrease of the differential stress by the static stress change of the Tohoku-Oki earthquake based on the background stress orientations of the finer grid result (Fig. 8a) by assuming that the principal stress axes did not rotate after the Tohoku-Oki earthquake. Signs of the differential stress change are shown in Fig. 9 by red and blue colors. Figure 9 indicates whether or not differential stress increased by the static stress change at each grid node. Although the computation result is somehow affected by our limited resolution of stress fields, we can see that differential stress increases only locally in some regions. Figure 9 shows the differential stress increased in the focal regions of the earthquake sequences N1, N2, S1, and S2. This suggests that the earthquake sequences N1, N2, S1, and S2 in these regions were caused by the increase in differential stress by the occurrence of the Tohoku-Oki earthquake due

to the local stress heterogeneity.

4. Discussion

4.1 Temporal variation in frictional strength due to upward fluid movement

The existence of the spatial stress heterogeneities in inland Tohoku can explain why the earthquake sequences in northern and southern Tohoku (N1, N2, N3, S1, and S2) were triggered by the Tohoku-Oki earthquake. However, it is difficult to explain the activation of the earthquake sequences in central Tohoku (C1, C2 and C3) (Fig. 10). Since they have reverse fault focal mechanisms with P-axes oriented WNW-ESE similarly to the typical focal mechanism in Tohoku, shear stress on the fault planes decreased by the WNW-ESE extension associated with the Tohoku-Oki earthquake (Yoshida et al., 2018a).

Previous studies suggest that those earthquake sequences in central Tohoku were activated in response to the increase in pore pressure due to the upwelling fluids facilitated by the WNW-ESE extension associated with the Tohoku-Oki earthquake (Terakawa et al., 2013; Okada et al., 2015; Yoshida et al., 2016b, 2017, 2018a and 2018b). Those earthquake sequences are characterized by the swarm-like seismicity pattern with a

distinct migration behavior of hypocenters, as summarized by Okada et al. (2015). Such migration behaviors of hypocenters are similar to the fluid-injection induced seismicity (e.g., Julian et al., 2010; Rutledge et al., 2004; Shapiro et al., 1997). Differential stress magnitude in inland Tohoku is estimated to be a few tens of MPa or so by recent studies based on the correlation of stress field with topography (Yoshida et al., 2015a) and with the static stress change by the recent large (~M7) inland earthquakes (Yoshida et al., 2014, 2015b, 2016c). Given that differential stress magnitude in Tohoku is as small as a few tens of MPa, pore pressure needs to be much higher than hydrostatic to cause earthquakes under expected effective normal stress at seismogeneic depth and the typical value of coefficient of friction obtained by laboratory experiments (e.g. Sibson, 1974). It should be noted that the differential stress magnitude of a few tens of MPa is much higher than 1 MPa estimated based on the stress rotation after the 2011 Tohoku-Oki earthquake in inland Tohoku (Yoshida et al., 2012), which was apparently obtained from ignoring the spatially heterogeneous stress field (Fig. 8a).

A plausible cause for the reduction in the frictional strength is increasing pore pressure (e.g., Hasegawa, 2017; Hubbert & Rubey, 1959; Miller, 2013; Nur & Booker, 1972; Rice, 1992; Sibson, 1992).

In fact, temporal variations in frictional strengths, stress drops, b-values, and

seismicity pattern have been detected for the Yamagata-Fukushima border earthquake swarm (C1), which can be explained by the temporal change in pore pressure in its source area (Yoshida et al., 2016b, 2017, 2018b). The source area of this swarm is located just beneath the late Miocene Ohtoge caldera and is related to the volcanic structure (Kanisawa et al., 2006; Yoshida et al., 2016b), which is believed to include shallow igneous bodies with hydrothermal fluids immediately below (Yoshida et al., 2005 and 2014). Precisely relocated hypocenters by Yoshida et al. (2018b) clearly show that they are concentrated on several discrete planes and migrate along those planes from deeper to shallower levels (Fig. 11).

Depth–time plots of hypocenters of events in the three earthquake sequences C1, C2, and C3 in central Tohoku (Fig. 12) clearly show hypocenters moved from deeper to shallower level in all the sequences. The initiations of the seismic activity of these swarms were delayed a few days to a few weeks after the occurrence of the Tohoku-Oki earthquake (Fig. 3). The delays of the initiation of seismicity, only observed in the earthquake sequences in central Tohoku, might have been necessary for the upwelling fluids to move and increase the pore pressure in their source areas to fulfill the failure criterion.

All these swarms are located near the ancient caldera structures (Kanisawa et al.,

2006; Yoshida et al., 2016b). High b-values were obtained all for these swarms ranging from 1.3-1.6 (Fig. 13d, e and f), which are significantly high compared to the other earthquake sequenses (Fig. 13a, b, c, g, and h) and the typical estimation value of ~0.8 in Tohoku (e.g., Cao & Gao, 2002), which might reflect high pore pressure in the source area as suggested from the observations of the fluid-injection induced seismicity (e.g., Wyss, 1978; Bachmann, 2012). Indeed, Yoshida et al. (2017) reported that b-value changes from 2 to 1 in the source area of the Yamagata-Fukushima border earthquake swarm in association with decreasing pore pressure.

These similarities support that all the three earthquake swarms in central Tohoku were caused by the increase in pore pressure due to upward fluid movements facilitated by the decrease in WNW-ESE compressional stress due to the Tohoku-Oki earthquake. Breaking of low-permeability seals due to the ground shaking might have helped fluid move to the shallower levels. The fluids permeated into several pre-existing planes, reduced the frictional strengths, and satisfied the failure criteria, causing the earthquake swarms despite the reduction in the Coulomb stress. The fluids probably further migrated upward along the planes, which is manifested as the hypocenters migrating along the planes.

Fluid movements after the Tohoku-Oki earthquake affected earthquake occurrences

not only in the central part of Tohoku. Kosuga et al. (2013) reported that the earthquake swarm in northern Tohoku (N1) also exhibits a distinct migration behavior of hypocenters. Namely, both the differential stress and the pore pressure increased in this cluster after the Tohoku-Oki earthquake. Delayed triggered swarms with the migration behaviors of hypocenters were also observed after the Mw 7.8 Dusky Sound and the Mw 7.1 Darfield earthquake in New Zealand probably due to the fluid diffusion (Boese et al., 2014). These observations suggest that the pore pressure change after the occurrence of a large earthquake more or less universally plays an important role for subsequent earthquake sequences in association with the stress change.

4.2 A possible cause of heterogeneity of stress field

We observed the spatial heterogeneities in stress field in inland Tohoku even before the Tohoku-Oki earthquake (Fig. 8b) based on the stress tensor inversion analyses. The stress tensor inversion methods (e.g., Gephart & Forsyth, 1984; Michael, 1987) were devised to avoid the effects of the bias in fault planes (McKenzie, 1969) by utilizing the diversity of focal mechanisms. It is still difficult, however, to completely distinguish the effect of the fault plane bias from the variations of stress field (Townend, 2006). In fact, estimation errors of focal mechanism lead to apparent diversity of focal mechanism.

Furthermore, even small earthquakes can perturb the nearby stress field, which violates the assumption of the uniform stress orientation in the considered volume. One way to remove this effect is the use of declustered seismicity catalogue as advocated by Martinez-Garzon et al. (2016b); however, this reduces the number of available focal mechanism data to examine the detailed spatial variation. Therefore, in this study, we have been focusing on a relatively large-scale pattern of stress fields and have discussed the variation in stress fields with such a length scale. Hypocenters of events with anomalous focal mechanisms that occurred after the Tohoku-Oki earthquake are concentrated at several locations in clusters (N1, N2, S1), rather than being distributed homogeneously throughout the Tohoku region (Fig. 2a), which suggests that the predominant length scales of the heterogeneity of stress field roughly correspond to those of the clusters (> 10 km).

To confirm the existence of the spatial heterogeneity in stress fields, we used the angle between the direction of the slip and the maximum resolved shear stress computed from the regional stress field (misfit angle). For that, we first performed the stress tensor inversion by assuming that the stress field is uniform in the entire Tohoku, and computed misfit angle of each focal mechanism. The obtained stress field shows the WNW-ESE compressional reverse faulting stress regime (Fig. 14a) with the mean misfit angle of

approximately 35° (Fig. 14b). We selected the fault plane from the two nodal planes as having the smaller misfit angle. We then computed the mean values of misfit angles at each grid node based on focal mechanism data used for the stress tensor inversions in Fig. 8. The spatial distribution of misfit angles in Fig. 14 (c) indicates a deviation of the stress field from the WNW-ESE compressional reverse faulting stress regime (Fig. 14a). The spatial variation is consistent with the stress tensor inversion results in Fig. 8(a). In particular, mean misfit angles are high in the focal regions of earthquakes that occurred after the 2011 Tohoku-Oki earthquake (N1, N2, N3 and S1), which confirms that these earthquakes occurred in regions with anomalous stress field.

One possible explanation of the local stress heterogeneities is the effect of the static stress change of large earthquakes that occurred previously. The static stress change of an earthquake can rotate the principal stress axes in and around the source region (e.g., Hardebeck & Hauksson, 2000; Wesson & Boyd, 2007), if magnitudes of deviatoric stress tensor components of the background stress field are small compared to those of the static stress change. The differential stress magnitude in inland Tohoku is estimated to be < ~ a few tens of MPa based on the correlation of orientations of the principal stress axes with the topography (Yoshida et al., 2015a). This value of the differential stress is similar to that estimated by Hasegawa et al. (2011) for the source area of the Tohoku-Oki earthquake

based on the stress rotation observed after the earthquake. Indeed, spatial heterogeneities in the stress orientations have been detected in the focal regions of the recent three large earthquakes in inland Tohoku: the 2003 M6.3 Northern Miyagi Prefecture earthquake (Yoshida et al., 2016c), the 2008 M7.2 Iwate-Miyagi Nairiku earthquake (Yoshida et al., 2014), and the 2011 M7.0 Fukushima-Hamadori earthquake (Yoshida et al., 2015b). The spatial patterns of the principal stress axes in their source areas after the mainshocks are well explained by the static stress change of those mainshocks, suggesting that the differential stress magnitude in inland Tohoku is very small (< a few ten MPa) and the effects of large earthquake can produce the spatial heterogeneities in stress orientations.

Conversely, if differential stress magnitude in Tohoku is small (less than a few tens of MPa), the principal stress axes should rotate by various effect such as effects of the topography and the static stress change of a large earthquake. The approximate focal regions of large (M>6.5) earthquakes that occurred in Tohoku before 1950 listed by Usami (2003) are shown in Fig. 8 (a) by circles. The focal regions indicated roughly correspond to the regions with anomalous stress orientations. This suggests the possibility that the stress axes locally rotated in these regions after the large earthquakes, and this time the earthquake sequences were triggered by the Tohoku-Oki earthquake because of the local increase in differential stress due to the stress heterogeneities thus produced.

The stress field in northern Tohoku is characterized by the WNW-ESE compression as well as the N-S compression depending on location (Fig. 8a). This suggests the existence of other causes of the regional stress in northern Tohoku besides the relative movement of the Pacific plate and the overriding plate. Seno (1999) assumed a higher magnitude of N-S compressional stress in central and eastern Japan than in western Japan because of the collision of the Izu Peninsula with central and eastern Japan from south (Matsuda, 1978). In fact, the orientation of $\sigma 1$-axis is rotated to NNW-SSE direction locally near the Izu Peninsula (Ukawa et al., 1982). The sliver motion of the Kuril fore-arc located just north (e.g., Kimura, 1986; Acocella et al., 2008) might not only sustain the collision force but also increase N-S compressional force in northern Tohoku. The gravitational collapse of the mountain range (Wang & He, 1999) might reduce the WNW-ESE compressional stress.

5. Conclusions

We examined the spatial variation in stress field in inland Tohoku to understand the triggering mechanisms of earthquake sequences by the 2011 Tohoku-Oki earthquake that occurred in the stress shadow. Focal mechanisms of shallow earthquakes in inland Tohoku are newly determined based on the P-wave first motion polarity data, and we inverted

them for the stress orientations.

The obtained spatial distribution of the stress orientation shows some variations in inland Tohoku even before the Tohoku-Oki earthquake. Earthquake clusters triggered by the Tohoku-Oki earthquake tend to correspond to the regions in which the orientations of the background stress field are locally similar to those of the static stress change of the earthquake. This observation suggests that those earthquake clusters were triggered by the local increase in shear stress due to the static stress change, which was caused by the spatial heterogeneity of the stress orientation, already existed before the Tohoku-Oki earthquake.

A few earthquake swarms, however, were triggered in central Tohoku where differential stress decreased by the static stress change of the Tohoku-Oki earthquake. All the earthquake swarms have notable characteristics including delays of initiation time of seismic activity by a few days to a few weeks, upward migrations of hypocenters along several thin planes, and high b-values. Such features are similar to the fluid-injection induced seismicity. The source regions of these earthquake swarms are located near the ancient caldera structures and the major geological boundaries (Yoshida et al., 2014). The swarm activities are probably triggered by the upward fluid movement along such pre-existing structures, which was facilitated by the WNW-ESE extension associated with the

Tohoku-Oki earthquake. These observations demonstrate that information about the temporal evolutions of stress and frictional strength are necessary to understand the triggering mechanism of earthquakes.

Acknowledgments

We would like to thank the editor Y. Ben-Zion, an associate editor, and two anonymous reviewers for their constructive comments which helped improve the manuscript. The figures in the present paper were created using GMT (Wessel and Smith, 1998). The present study was partly supported by MEXT KAKENHI (No. 26109002).

References

Acocella, V., Yoshida, T., Yamada, R. and Funiciello, F. (2008). Structural control on late Moicene to Quaternary volcanism in the NE Honshu arc, Japan. Tectonics, 27, TC5008, doi:10.1029/2008TC002296.

Allmann, B. P., & Shearer, P. M. (2009). Global variations of stress drop for moderate to large earthquakes. Journal of Geophysical Research: Solid Earth, 114(1), 1–22. https://doi.org/10.1029/2008JB005821

Asano, Y., T. Saito, Y. Ito, K. Shiomi, H. Hirose, T. Matsumoto, S. Aoi, S. Hori and S. Sekiguchi (2011), Spatial distribution and focal mechanisms of aftershocks of the 2011 off the Pacific Coast of Tohoku Earthquake, Earth Planets Space, 63, 669–673, http://dx.doi.org/10.5047/eps.2011.06.016.

Bachmann, C. E., S. Wiemer, B. P. Goertz-Allmann, and J. Woessner (2012), Influence of pore-pressure on the event-size distribution of induced earthquakes, Geophys. Res. Lett., 39(9), 1–7, doi:10.1029/2012GL051480.

Boese, C. M., Jacobs, K. M., Smith, E. G. C., Stern, T. A., & Townend, J. (2014). Background and delayed-triggered swarms in the central Southern Alps, South Island, New Zealand. Geochemistry, Geophysics, Geosystems, 15(4), 945–964.

Brown, L., Wang, K., & Sun, T. (2015). Static stress drop in the Mw 9 Tohoku-oki earthquake: Heterogeneous distribution and low average value. Geophys. Res. Lett., 42(24), 10595–10600. https://doi.org/10.1002/2015GL066361

Cao, Aimin, and Stephen S. Gao, (2002), Temporal Variation of Seismic B-Values beneath Northeastern Japan Island Arc, Geophysical Research Letters 29 (9), http://onlinelibrary.wiley.com/doi/10.1029/2001GL013775/full.

Chiba, K., Iio, Y., Fukahata, Y., 2013. Detailed stress fields in the focal region of the 2011 off the Pacific coast of Tohoku Earthquake—Implication for the distribution of moment release—. Earth, Planets Sp. 64, 1157–1165. doi:10.5047/eps.2012.07.008

Enescu, B., Aoi, S., Toda, S., Suzuki, W., Obara, K., Shiomi, K., Takeda, T., 2012. Stress perturbations and seismic response associated with the 2011 M9.0 Tohoku-oki earthquake in and around the Tokai seismic gap, central Japan. Geophys. Res. Lett. 39, 10‑15. doi:10.1029/2012GL051839

Fukuyama, E., Ishida, M., Dreger, D. S., & Kawai, H. (1998). Automated seismic moment tensor determination by using on-line broadband seismic waveforms. Zisin, 51(1), 149–156.

Fukuyama, E., & Dreger, D. (2003). Performance test of an automated moment tensor

determination system for the future “Tokai” earthquake. Earth, Planets and Space, 52(6), 383–392. https://doi.org/10.1186/BF03352250.

Frohlich, C. (1992). Triangle diagrams: ternary graphs to display similarity and diversity of earthquake focal mechanisms. Physics of the Earth and Planetary Interiors, 75(1–3), 193–198. https://doi.org/10.1016/0031-9201(92)90130-N.

Gephart, J. W., and D. W. Forsyth (1984), An improved method for determining the regional stress tensor using earthquake focal mechanism data: Application to the San Fernando earthquake sequence, J. Geophys. Res., 89, 9305-9320, doi: 10.1029/JB089iB11p09305.

Hainzl, S., and T. Fischer (2002), Indications for a successively triggered rupture growth underlying the 2000 earthquake swarm in Vogtland/NW Bohemia, J. Geophys. Res. Solid Earth, 107(B12), 1–9, doi:10.1029/2002JB001865.

Hardebeck, J. L. and E. Hauksson (2001), Crustal stress field in Southern California and its implications for fault mechanics, J. Geophys. Res., 106, 21, 859–21, 882, doi:10.1029/2001JB000292.

Hardebeck, J. L. and A. J. Michael (2006), Damped regional-scale stress inversions: Methodology and examples for Southern California and the Coalinga

aftershock sequence, J. Geophys. Res., 111, B11310, doi:10.1029/2005JB004144.

Hardebeck, J. L. and P. M. Shearer (2002), A new method for determining first-motion focal mechanisms, Bull. Seismol. Soc. Am., 92, 2264–2276, doi:10.1785/0120010200.

Hardebeck, J. L. (2012), Coseismic and postseismic stress rotations due to great subduction zone earthquakes, Geophys. Res. Lett., 39, L21313, doi:10.1029/2012GL053438.

Hasegawa, A., 2017. Role of H2O in Generating Subduction Zone Earthquakes. Monogr. Environ. Earth Planets 5, 1–34. doi:10.5047/meep.2017.00501.0001

Hasegawa, A., Horiuchi, S., Umino, N., 1994. Seismic structure of the northeastern Japan convergent margin: A synthesis. J. Geophys. Res. Solid Earth 99, 22295–22311. doi:doi: 10.1029/93JB02797

Hasegawa, A., Yoshida, K., 2015. Preceding seismic activity and slow slip events in the source area of the 2011 Mw 9.0 Tohoku-Oki earthquake: a review. Geosci. Lett. 2, 6. doi:10.1186/s40562-015-0025-0

Hasegawa, A., Yoshida, K., Asano, Y., Okada, T., Iinuma, T., Ito, Y., 2012. Change in

stress field after the 2011 great Tohoku-Oki earthquake. Earth Planet. Sci. Lett. 355–356, 231–243. doi:10.1016/j.epsl.2012.08.042

Hubbert, M., Rubey, W., 1959. Role of fluid pressure in mechanics of overthrust faulting I. Mechanics of fluid-filled porous solids and its application to overthrust faulting. Geol. Soc. Am. Bull. 70, 115–166.

Iinuma, T., Hino, R., Kido, M., 2012. Coseismic slip distribution of the 2011 off the Pacific Coast of Tohoku Earthquake (M9. 0) refined by means of seafloor geodetic data. J. Geophys. Res. Solid Earth 117, B07409. doi:10.1029/2012JB009186

Imanishi, K., R. Ando and Y. Kuwahara (2011), Unusual shallow normal-faulting earthquake sequence in compressional northeast Japan activated after the 2011 off the Pacific coast of Tohoku earthquake, Geophys. Res. Lett., 39, L09306, doi:10.1029/2012GL051491.

Ishibe, T., Shimazaki, K., Satake, K., & Tsuruoka, H. (2011). Change in seismicity beneath the Tokyo metropolitan area due to the 2011 off the Pacific coast of Tohoku Earthquake. Earth, Planets and Space, 63(7). https://doi.org/10.5047/eps.2011.06.001.

Julian, B.R., Foulger, G.R., Monastero, F.C., Bjornstad, S., 2010. Imaging hydraulic

fractures in a geothermal reservoir. Geophys. Res. Lett. 37, 1–5. doi:10.1029/2009GL040933.

Kanisawa, S., Otsuki, K., Ehiro, M., Yoshida, T., Kazama, M., Kano, K., Takarada, S., Wakita, K., Kyogoku, M., Nakayama, M., Shikama, S., Koyama, T. and Miura, A. (2006), Geology of NE Honshu for construction engineers (with digital geological map of Tohoku district, Japan (1:200,000)) (in Japanese), report, 408pp., Tohoku Constr. Assoc., Sendai, Japan.

Kato, T., G. S. El-Fiky, E. N. Oware and S. Miyazaki (1998), Crustal strains in the Japanese Islands as deduced from dense GPS array, Geophys. Res. Lett., 25(18), 3445–3448, doi:10.1029/98GL02693.

Kato, A., S. Sakai and K. Obara (2011), A normal-faulting seismic sequence triggered by the 2011 off the Pacific coast of Tohoku earthquake: Wholesale stress regime changes in the upper plate, Earth Planets Space, 63, 745–748, doi:10.5047/eps.2011.06.014.

Kato, A., & Igarashi, T. (2012). Regional extent of the large coseismic slip zone of the 2011 Mw 9.0 Tohoku-Oki earthquake delineated by on-fault aftershocks. Geophysical Research Letters, 39(15), 2–7. https://doi.org/10.1029/2012GL052220

Kato, A., Fukuda, J., Obara, K. (2013), Response of seismicity to static and dynamic stress changes induced by the 2011 M9.0 Tohoku-Oki earthquake. Geophys. Res. Lett. 40, 3572–3578. doi:10.1002/grl.50699

Kosuga, M., 2014. Seismic activity near the Moriyoshi-zan volcano in Akita Prefecture, northeastern Japan: implications for geofluid migration and a midcrustal geofluid reservoir. Earth, Planets Sp. 66, 77. doi:10.1186/1880-5981-66-77

Lengliné, O., Enescu, B., Peng, Z., Shiomi, K., 2012. Decay and expansion of the early aftershock activity following the 2011, Mw 9.0 Tohoku earthquake. Geophys. Res. Lett. 39, 6–11. doi:10.1029/2012GL052797.

Lund, B. and J. Townend (2007), Calculating horizontal stress orientations with full or partial knowledge of the tectonic stress tensor, Geophys. J. Int., doi:10.1111/j.1365–246X.2007.03468.x.

Mallman, E. P., & Zoback, M. D. (2007). Assessing elastic Coulomb stress transfer models using seismicity rates in southern California and southwestern Japan. Journal of Geophysical Research, 112(B3), 37.

Martínez-Garzón, P., Kwiatek, G., Bohnhoff, M., & Dresen, G. (2016a). Impact of fluid injection on fracture reactivation at The Geysers geothermal field. J. Geophys. Res. Solid Earth, 121, 7432–7449.

Martínez-Garzón, P., & Ben‐Zion, Y. (2016b). A refined methodology for stress inversions of earthquake focal mechanisms. J. Geophys. Res. Solid Earth, 121, 8666–8687, doi:10.1002/2016JB013493.

Matsuda, T., & Uyeda, S. (1971). On the pacific-type orogeny and its model - extension of the paired belts concept and possible origin of marginal seas. Tectonophysics, 11(1), 5–27. https://doi.org/10.1016/0040-1951(71)90076-X/

McKenzie,D., (1969). The relationship between fault plane solutions for earthquakes and the directions of the principal stresses, Bull. Seism. Soc. Am., 59, 591–601.

Michael, A. J. (1984), Determination of stress from slip data; faults and folds, J. Geophys. Res. 89, 11,517–11,526, doi: 10.1029/JB089iB13p11517.

Michael, A. J. (1987), Use of focal mechanisms to determine stress: A control study, J. Geophys. Res., 92, 357– 368, doi: 10.1029/JB092iB01p00357.

Miller, S. A. (2013), The role of fluids in tectonic and earthquake processes. Adv Geophys., 54, 1–46.

Miura, S., T. Sato, K. Tachibana, Y. Satake and A. Hasegawa (2002), Strain accumulation in and around Ou Backbone Range, northeastern Japan as

observed by a dense GPS network, Earth Planets Space, 54, 1071–1076.

Miyazawa, M., 2011. Propagation of an earthquake triggering front from the 2011 Tohoku-Oki earthquake. Geophys. Res. Lett. 38, 1–6. doi:10.1029/2011GL049795

Nakajima, J., Yoshida, K., Hasegawa, A., 2013. An intraslab seismic sequence activated by the 2011 Tohoku-oki earthquake: Evidence for fluid-related embrittlement. J. Geophys. Res. Solid Earth 118, 3492–3505. doi:10.1002/jgrb.50246

Nakamura, K., & Uyeda, S. (1980). Stress gradient in arc–back arc regions and plate subduction. Journal of Geophysical Research, 85(B11), 6419. https://doi.org/10.1029/JB085iB11p06419

Nakamura, W., N. Uchida, and T. Matsuzawa, Spatial distribution of the faulting types of small earthquakes around the 2011 Tohoku-oki earthquake: A comprehensive search using template events, J. Geophys. Res., 121, doi:10.1002/2015JB012584, 2016

Nur, A., and J. R. Booker (1972), Aftershocks caused by pore fluid flow?, Science, 175(4024), 885–887, doi:10.1126/science.175.4024.885.

Okada, Y., 1992. Internal deformation due to shear and tensile faults in a half-space.

Bull. Seismol. Soc. Am. 82, 1018–1040.

Okada, T., Yoshida, K., Ueki, S., Nakajima, J., Uchida, N., Matsuzawa, T., … Hasegawa, A. (2011). Shallow inland earthquakes in NE Japan possibly triggered by the 2011 off the Pacific coast of Tohoku Earthquake. Earth, Planets and Space, 63(7), 749–754. https://doi.org/10.5047/eps.2011.06.027

Okada, T., Matsuzawa, T., Umino, N., Yoshida, K., Hasegawa, A., Takahashi, H., Yamada, T., Kosuga, M., Takeda, T., Kato, A., Igarashi, T., Obara, K., Sakai, S., Saiga, A., Iidaka, T., Iwasaki, T., Hirata, N., Tsumura, N., Yamanaka, Y., Terakawa, T.,

Oth, A. (2013). On the characteristics of earthquake stress release variations in Japan. Earth and Planetary Science Letters, 377–378, 132–141. https://doi.org/10.1016/j.epsl.2013.06.037

Nakamichi, H., Okuda, T., Horikawa, S., Katao, H., Miura, T., Kubo, A., Matsushima, T., Goto, K., Miyamachi, H., 2015. Hypocenter migration and crustal seismic velocity distribution observed for the inland earthquake swarms induced by the 2011 Tohoku-Oki earthquake in NE Japan: implications for crustal fluid distribution and crustal permeability. Geofluids 15, 293–309. doi:10.1111/gfl.12112.

Rice, J. R. (1992), Fault stress states, pore pressure distributions, and the weakness of the San Andreas Fault, In Evans, B., and T. F. Wong, eds., Fault mechanics and transport properties of rocks, New York, Academic Press, p. 475–503.

Rutledge, J.T., Phillips, W.S., Mayerhofer, M.J., 2004. Faulting induced by forced fluid injection and fluid flow forced by faulting: An interpretation of hydraulic-fracture microseismicity, Carthage Cotton Valley gas field, Texas. Bull. Seismol. Soc. Am. 94, 1817–1830. doi:10.1785/012003257.

Sagiya, T., Miyazaki, S. and Tada, T. (2000), Continuous GPS array and present-day crustal deformation of Japan, Pure Appl. Geophys, 157, 2303–2322.

Seno, T. (1999). Syntheses of the regional stress fields of the Japanese islands. Island Arc, 8(1), 66–79. https://doi.org/10.1046/j.1440-1738.1999.00225.x

Shapiro, S.A., Huenges, E., Borm, G., 1997. Estimating the crust permeability from fluid-injection-induced seismic emission at the KTB site. Geophys. J. Int. 131, F15–F18. doi:10.1111/j.1365-246X.1997.tb01215.x.

Shimojo, K., Enescu, B., Yagi, Y., Takeda, T., 2014. Fluid-driven seismicity activation in northern Nagano region after the 2011 M9.0 Tohoku-oki earthquake. Geophys. Res. Lett. 41, 7524–7531. doi:10.1002/2014GL061763

Sibson, R. H. (1990). Rupture nucleation on unfavorably oriented faults. Bulletin of the

Seismological Society of America, 80(6), 1580–1604. https://doi.org/10.1021/jp111520r

Sibson, R. (1992), Implications of fault-valve behaviour for rupture nucleation and recurrence, Tectonophysics, 211(1–4), 283–293, doi:10.1016/0040-1951(92)90065-E.

Simpson, R. W., and P. A. Reasenberg, Earthquake-induced static- stress changes on central California faults, U.S. Geol. Surv. Prof. Pap., 1550-F, 55-89, 199.

Smith, D. E., & Dieterich, J. H. (2010). Aftershock Sequences Modeled with 3-D Stress Heterogeneity and Rate-State Seismicity Equations: Implications for Crustal Stress Estimation. Pure and Applied Geophysics, 167(8–9), 1067–1085. https://doi.org/10.1007/s00024-010-0093-1

Suwa, Y., Miura, S., Hasegawa, A., Sato, T., & Tachibana, K. (2006). Interplate coupling beneath NE Japan inferred from three-dimensional displacement field. Journal of Geophysical Research: Solid Earth, 111(4), 1–12. https://doi.org/10.1029/2004JB003203

Suzuki, Y., S. Toda, K. Yoshida, and T. Okada (2014), Local receiver fault dependency of seismicity shut down in the 2011 Tohoku-oki stress shadow, In AGU Fall Meeting, San Francisco, Abstracts (S23A–4473).

Terakawa T. and M. Matsu'ura (2010), The 3-D tectonic stress fields in and around Japan inverted from centroid moment tensor data of seismic events, Tectonics, 29, TC6008, doi:10.1029/2009TC002626.

Terakawa, T., Hashimoto, C., Matsu'ura, M., 2013. Changes in seismic activity following the 2011 Tohoku-oki earthquake: Effects of pore fluid pressure. Earth Planet. Sci. Lett. 365, 17–24. doi:10.1016/j.epsl.2013.01.017

Toda, S., Stein, R.S., Lin, J., 2011. Widespread seismicity excitation throughout central Japan following the 2011 M=9.0 Tohoku earthquake and its interpretation by Coulomb stress transfer. Geophys. Res. Lett. 38, 1–5. doi:10.1029/2011GL047834.

Townend, J. (2006). What do faults feel? Observational constraints on the stresses acting on seismogenic faults. In R. Abercrombie, A. McGarr, H. Kanamori & G. Di Toro (Eds.), Earthquakes: Radiated Energy and the Physics of Faulting (AGU Monograph Series Vol. 170, pp. 313–327). Washington D.C., USA: American Geophysical Union.

Townend, J., & Zoback, M. D. (2001). Implications of earthquake focal mechanisms for the frictional strength of the San Andreas fault system. Geological Society, London, Special Publications, 186(1), 13–21.

Townend, J., and M. D. Zoback (2006), Stress, strain, and mountain building in central Japan, J. Geophys. Res., 111, B03411, doi:10.1029/2005JB003759.

Ukawa, M. (1982). Lateral stretching of the philippine sea plate subducting along the nankai-suruga trough. Tectonics, 1(6), 543–571. https://doi.org/10.1029/TC001i006p00543

Usami, T. (2003), A catalogue of disastrous earthquakes in Japan, (in Japanese) updated edition, University of Tokyo Press. (728pp.).

Wang, K., & He, J. (1999). Mechanics of low-stress forearcs: Nankai and Cascadia. Journal of Geophysical Research, [Solid Earth], 104(B7), 15191–15205.

Wessel, P., and W. H. F. Smith (1998), New, improved version of the Generic Mapping Tools released, Eos Trans. AGU, 79, 579.

Wesson, R. L., and O. S. Boyd (2007), Stress before and after the 2002 Denali fault earthquake, Geophys. Res. Lett., 34, L07303, doi:10.1029/2007GL029189.

Wyss, M. (1973). Towards a Physical Understanding of the Earthquake Frequency Distribution. Geophysical Journal of the Royal Astronomical Society, 31(4), 341–359. https://doi.org/10.1111/j.1365-246X.1973.tb06506.x.

Yoshida, K., & Hasegawa, A. (2018a). Sendai-Okura earthquake swarm induced by the 2011 Tohoku-Oki earthquake in the stress shadow of NE Japan: Detailed

fault structure and hypocenter migration. Tectonophysics, 733, 132–147.

Yoshida, K., & Hasegawa, A. (2018b). Hypocenter Migration and Seismicity Pattern Change in the Yamagata-Fukushima Border, NE Japan, Caused by Fluid Movement and Pore Pressure Variation. Journal of Geophysical Research, [Solid Earth], 95, 664.

Yoshida, K., A. Hasegawa, T. Okada, T. Iinuma, Y. Ito and Y. Asano (2012), Stress before and after the 2011 great Tohoku-oki earthquake and induced earthquakes in inland areas of eastern Japan, Geophys. Res. Lett., 39, L03302, doi:10.1029/2011GL049729.

Yoshida, K., A. Hasegawa, T. Okada, and T. Iinuma (2014), Changes in the stress field after the 2008 M7.2 Iwate-Miyagi Nairiku earthquake in northeastern Japan, J. Geophys. Res. Solid Earth, 119(12), 9016–9030, doi:10.1002/2014JB011291.

Yoshida, K., Hasegawa, A., Okada, T., (2015a), Spatial variation of stress orientations in NE Japan revealed by dense seismic observations. Tectonophysics 647–648, 63–72. doi:10.1016/j.tecto.2015.02.013.

Yoshida, K., Hasegawa, A., & Okada, T. (2015b), Spatially heterogeneous stress field in the source area of the 2011 Mw 6.6 Fukushima-Hamadori earthquake, NE

Japan, probably caused by static stress change. Geophysical Journal International, 201(2), 1062–1071. https://doi.org/10.1093/gji/ggv068.

Yoshida, K., Pulido, N., & Fukuyama, E. (2016a). Unusual stress rotations within the Philippines possibly caused by slip heterogeneity along the Philippine fault: STRESS FIELDS IN THE PHILIPPINES. Journal of Geophysical Research, [Solid Earth], 121(3), 2020–2036.

Yoshida, K., Hasegawa, A., Yoshida, T., (2016b), Temporal variation of frictional strength in an earthquake swarm in NE Japan caused by fluid migration. J. Geophys. Res. Solid Earth. doi:10.1002/2015JB012352.Received

Yoshida, K., A. Hasegawa, and T. Okada (2016c), Heterogeneous stress field in the source area of the 2003 M6.4 Northern Miyagi Prefecture, NE Japan, earthquake, *Geophys. J. Int.*, 206(1), 408–419, doi:10.1093/gji/ggw160.

Yoshida, K., Saito, T., Urata, Y., Asano, Y., & Hasegawa, A. (2017). Temporal Changes in Stress Drop, Frictional Strength, and Earthquake Size Distribution in the 2011 Yamagata-Fukushima, NE Japan, Earthquake Swarm, Caused by Fluid Migration: Changes in Stress Drop and B-Value. Journal of Geophysical Research, [Solid Earth], 122(12), 10,379–10,397.

Yoshida, T., J. Kimura, R. Yamada, V. Acocella, H. Sato, D. Zhao, J. Nakajima, A.

Hasegawa, T. Okada, S. Honda, M. Ishikawa, O. D. A. Prima, T. Kudo, B. Shibazaki, A. Tanaka and T. Imaizumi (2014), Evolution of late Cenozoic magmatism and the crust-mantle structure in the NE Japan Arc, Geol. Soc. Spec. Publ., 385, 335–387, doi:10.1144/SP385.15.

Yoshida, T., Nakajima, J., Hasegawa, A., Sato, H., Nagahashi, Y., Kimura, J., Tanaka, A., Prima, O.D.A. and Ohguchi, T. (2005), Evolution of late Cenozoic magmatism in the NE Honshu Arc and its relation to the crust-mantle structures. Quaternary Research, 44, 195-216 [in Japanese with English abstract].

Yoshida, T. (2017) Basic structure of Tohoku District (Chapter 2) in Edited by Yoshida, T. et al., Regional Geology of Japan 2, Tohoku District. Asakura Publishing Co. Ltd., 7-103. (in Japanese)

Yukutake, Y., Honda, R., Harada, M., Aketagawa, T., Ito, H., Yoshida, A., 2011b. Remotely-triggered seismicity in the Hakone volcano following the 2011 off the Pacific coast of Tohoku Earthquake. Earth, Planets Sp. 63, 737–740. doi:10.5047/eps.2011.05.004

Figure 1. Hypocenter distribution of shallow earthquakes ($z < 40$ km) that occurred after the 2011 Tohoku-Oki earthquake in the overriding plate. Dots show hypocenters of earthquakes listed in the JMA unified catalogue during the four-year period from March 11, 2011 with the JMA magnitude equal to or greater than 1.5. In this study, we focus on inland earthquakes shown by black colors. Other earthquakes are also shown by green. The rectangle with broken lines indicates the target region of this study. The black contours show the coseismic slip distribution of the Tohoku-Oki earthquake determined by Iinuma et al. (2012). Red and blue arrows show the orientations of the maximum principal stress ($\sigma 1$) axis and the minimum principal stress ($\sigma 3$) axis, respectively, at 10 km depth caused by the static stress change due to the Tohoku-Oki earthquake based on the elastic dislocation model of Okada (1992). The length of arrows varies according to the steepness of the plunge (i.e., shorter arrows are more steeply inclined). NA: North American plate, PA: Pacific plate. The arrow indicates the plate convergence direction.

Figure 2. Seismicity before and after the 2011 Tohoku-Oki earthquake. (a) Shallow earthquakes ($z < 40$ km) after the Tohoku-Oki earthquake (2011/3/11-2012). Hypocenters are shown by red circles. (b) Shallow earthquakes before (1997-

2011/3/11) the Tohoku-Oki earthquake are plotted over those after (2011/3/11-2012) the earthquake. Hypocenters are shown by gray circles (before) and red circles (after). The rectangles denote focal regions of intense seismicity after the earthquake. Major geological boundaries are shown by broken curves (Yoshida et al., 2014). (c) Space-time plot of earthquakes before and after the Tohoku-Oki earthquake in inland Tohoku. The occurrence time is plotted against latitude by black dots for 300 day periods before and after the Tohoku-Oki earthquake.

Figure 3. Temporal distributions of earthquake number for 150 day period before and after the Tohoku-Oki earthquake for eight earthquake clusters indicated in Fig. 2 (b). Cut off magnitude was set at 2.0. The blue curves show the cumulative number of earthquakes.

Figure 4. Distributions of P- and T-axes of focal mechanisms before and after the Tohoku-Oki earthquake. Focal mechanism data are the same as those in Yoshida et al. (2012) and Hasegawa et al. (2012). P-axes before and after the earthquake are shown in (a) and (b), respectively. T-axes before and after the earthquake are shown in (c) and (d), respectively. Red, green, blue, and black colors show reverse faulting,

strike-slip faulting, normal faulting and odd type, respectively, based on the classification of Frohlich (1992). Data periods of Yoshida et al. (2012) and Hasegawa et al. (2012) are from 1997 to 20 July 2011 and from 2003 to 30 September 2011, respectively.

Figure 5. Principal stress axes (a) before and (b) after the Tohoku-Oki earthquake and (c) the static stress change of the earthquake in the overriding plate. Stress tensor inversion results and the static stress change by Yoshida et al. (2012) and Hasegawa et al. (2012) are shown by arrows. Red and blue arrows show $\sigma 1$ and $\sigma 3$ axes, respectively. Dark arrows in (c) highlight the results in the region where the stress tensor inversion is performed both before and after the Tohoku-Oki earthquake. The length of arrows varies according to the steepness of the plunge (i.e., shorter arrows are more steeply inclined).

Figure 6. A schematic illustration explaining the drastic change of focal mechanisms after the earthquake by the spatial change in stress field. Orientations of principal stress axis are represented by beach-balls. P-, B-, and T-axes corresponds to $\sigma 1$, $\sigma 2$, and $\sigma 3$ axes, respectively. (a) Stress field before the earthquake. (b) Static stress

change caused by the earthquake. (c) Resultant stress field. Red and blue indicate increase and decrease in differential stress, respectively.

Figure 7. Distribution of focal mechanism data used in this study. Red, green, blue, and black beach-balls show reverse faulting, strike-slip faulting, normal faulting, and odd type, respectively, based on the classification of Frohlich (1992).

Figure 8. Stress field before the Tohoku-Oki earthquake and the static stress change. (a) Orientations of the observed maximum horizontal compressive stress σ_{HMAX} measured in degrees clockwise from north determined based on the first approach described in Section 3.2. Orientations of σ_{HMAX} are shown by the color scale at the left top. (b) Orientations of the best fit σ_1 and σ_3 axes projected onto a gridded horizontal plane determined based on the second approach described in Section 3.2. (c) Orientations of σ_1 and σ_3 axes of the static stress change of the Tohoku-Oki earthquake at 20 km depth. In Fig. 8(b) and Fig. 8(c), σ_1 and σ_3 axes are indicated by red and blue arrows, respectively, at each grid reference. The length of arrows varies according to the steepness of the plunge (i.e., shorter arrows are more steeply

inclined).

Figure 9. Spatial distribution of increase or decrease of differential stress by the static stress change of the Tohoku-Oki earthquake. Differential stress change is shown by the color scale.

Figure 10. Hypocenter distribution of earthquakes in central Tohoku before and after the Tohoku-Oki earthquake. Gray and blue circles show hypocenters before and after the earthquake, respectively. Beach-balls show focal mechanisms of events in the earthquake sequences C1, C2, and C3 listed in the F-net moment tensor catalogue (Fukuyama et al., 1998, 2003) and the JMA catalogue. Major geological boundaries are shown by broken curves (Yoshida et al., 2014).

Figure 11. Hypocenter distribution of the earthquake swarm C1 in the Yamagata-Fukushima border. Hypocenters were relocated by Yoshida et al. (2018b). (a) Map view showing hypocenter migration. Dots show hypocenters of earthquakes for the period of 800 days from the beginning of the swarm activity. Elapsed time after the Tohoku-Oki earthquake is shown by the color scale. The thin broken line denotes the

border line between Yamagata and Fukushima prefectures. The thick broken line denotes the rim of the Ohtoge caldera (Kanisawa et al., 2006). (b)-(f) Cross-sectional views showing hypocenter migration along five discrete planes in the western cluster of this earthquake swarm. Hypocenters are shown separately on the five discrete planes plotted on a vertical cross section along the solid line shown in (a). Color scale shows the sequence of earthquake occurrence ordered by time. Sizes of circles correspond to fault diameter assuming a stress drop of 10 MPa. Gray circles show hypocenters of other earthquakes.

Figure 12. Depth–time plots of the hypocenters of events in the three earthquake sequences in central Tohoku for (a) the Yamagata-Fukushima border swarm C1; (b) the Sendai-Okura swarm C2; (c) the Yamagata swarm C3.

Figure 13. Magnitude-frequency distributions of earthquakes in the earthquake clusters. Black dots indicate the cumulative number of earthquakes. Red broken lines show the best-fit Gutenberg-Richter relation. Blue inverted triangles indicate the cut-off magnitude for the fitting of the Gutenberg-Richter relation.

Figure 14. (a) Principal stress axis orientations determined by the stress tensor inversion based on all the focal mechanism data in Tohoku. Red, green, and blue circles show σ1, the σ2 , and σ3-axes, respectively. Circles denote the best-fit solution. (b) Histogram showing the frequency distribution of misfit angles. (c) Spatial distribution of the mean values of misfit angles of focal mechanisms. The mean values are plotted at the same grids used in the stress tensor inversion of Fig. 8(a).

Figure S1. Examples of focal mechanism solutions determined by the present study. (a) Focal mechanisms evaluated as rank A and (b) those as rank B by the criteria of Hardebeck and Shearer (2002). The frequency distributions of the number of polarity data used for the determinations are shown in (c) for focal mechanisms with rank A and in (e) for those with rank B. The frequency distributions of average RMS angular differences between the best solutions to their acceptable solutions are shown in (d) for focal mechanisms with rank A and in (f) for those with rank B.

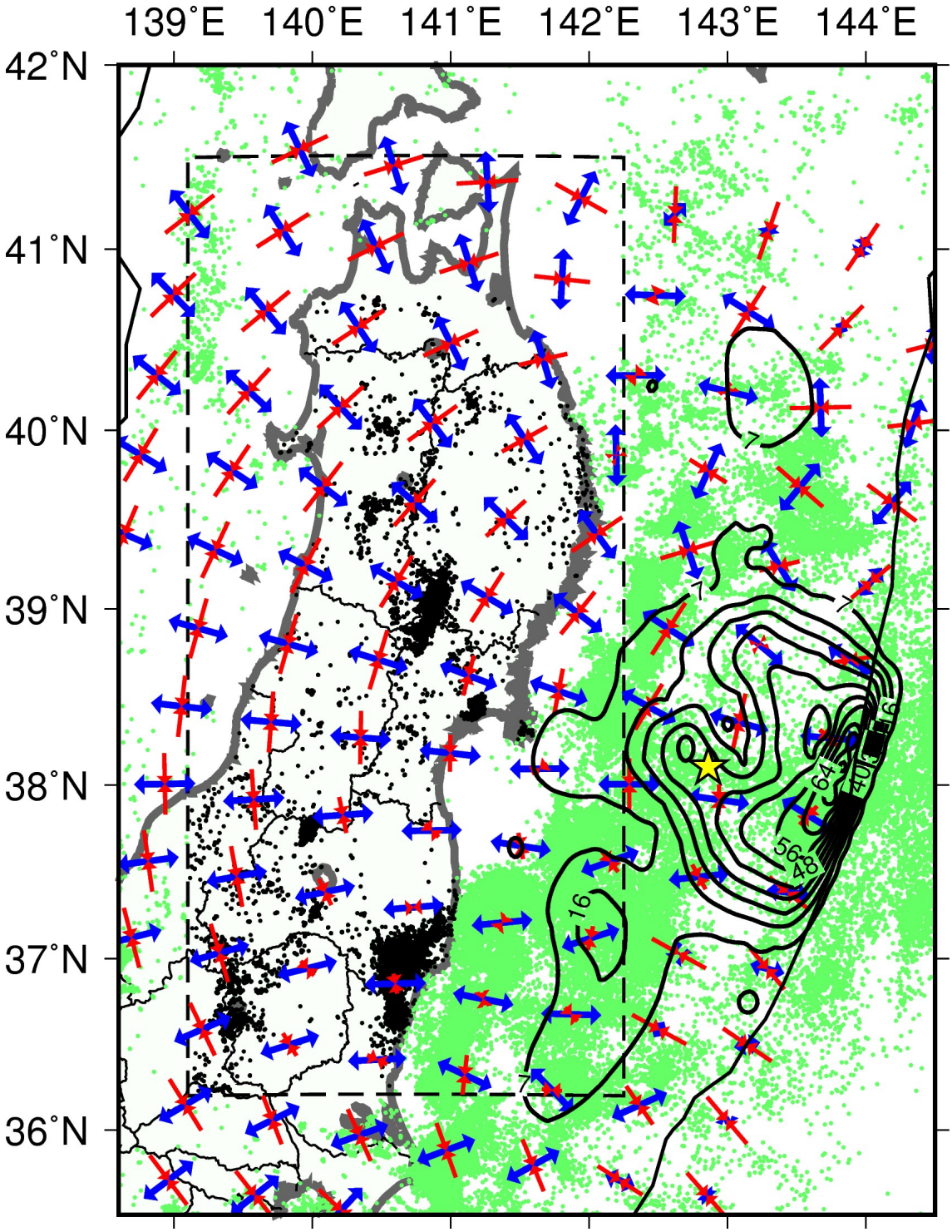
139˚E
140˚E
141˚E
142˚E
143˚E
144˚E
42˚N
41˚N
40˚N
39˚N
38˚N
37˚N
36˚N
7
16
40
48
56
64

Figure 1

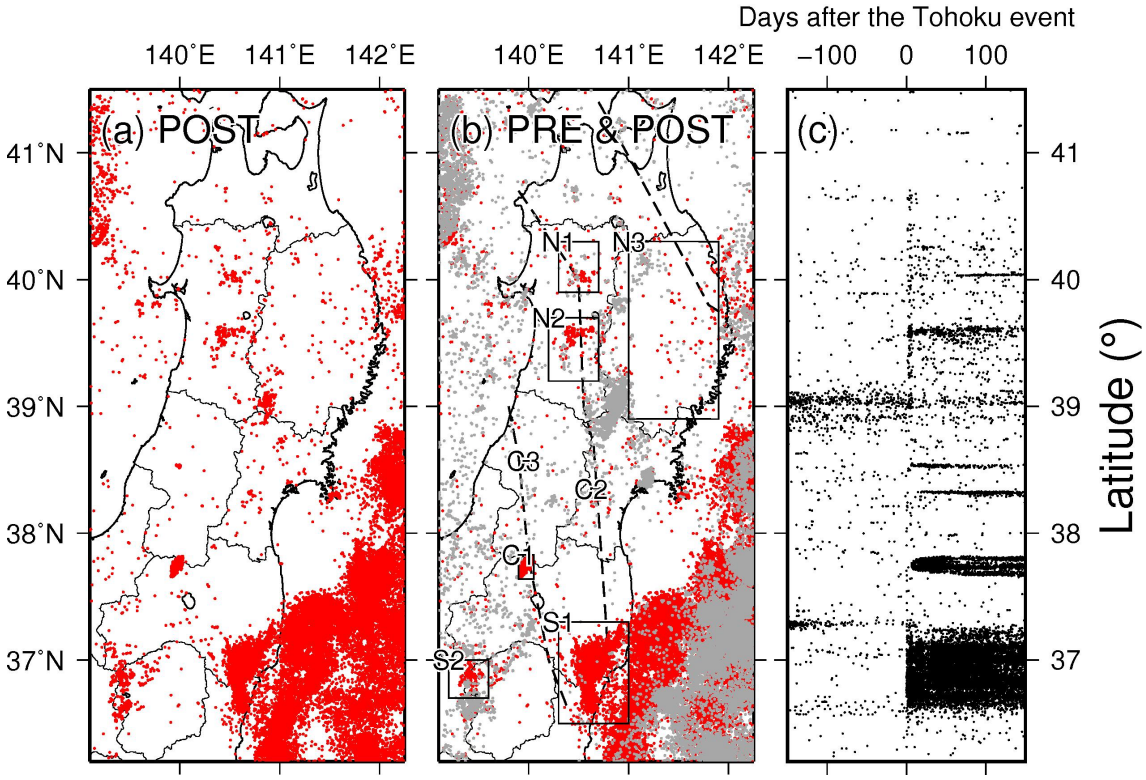
Days after the Tohoku event
140˚E
141˚E
142˚E
−100
0
100
(a) POST
(b) PRE & POST
(c)
41˚N
40˚N
39˚N
38˚N
37˚N
N1
N2
N3
C1
C2
C3
S1
S2
41
40
39
38
37
Latitude (°)

Figure 2

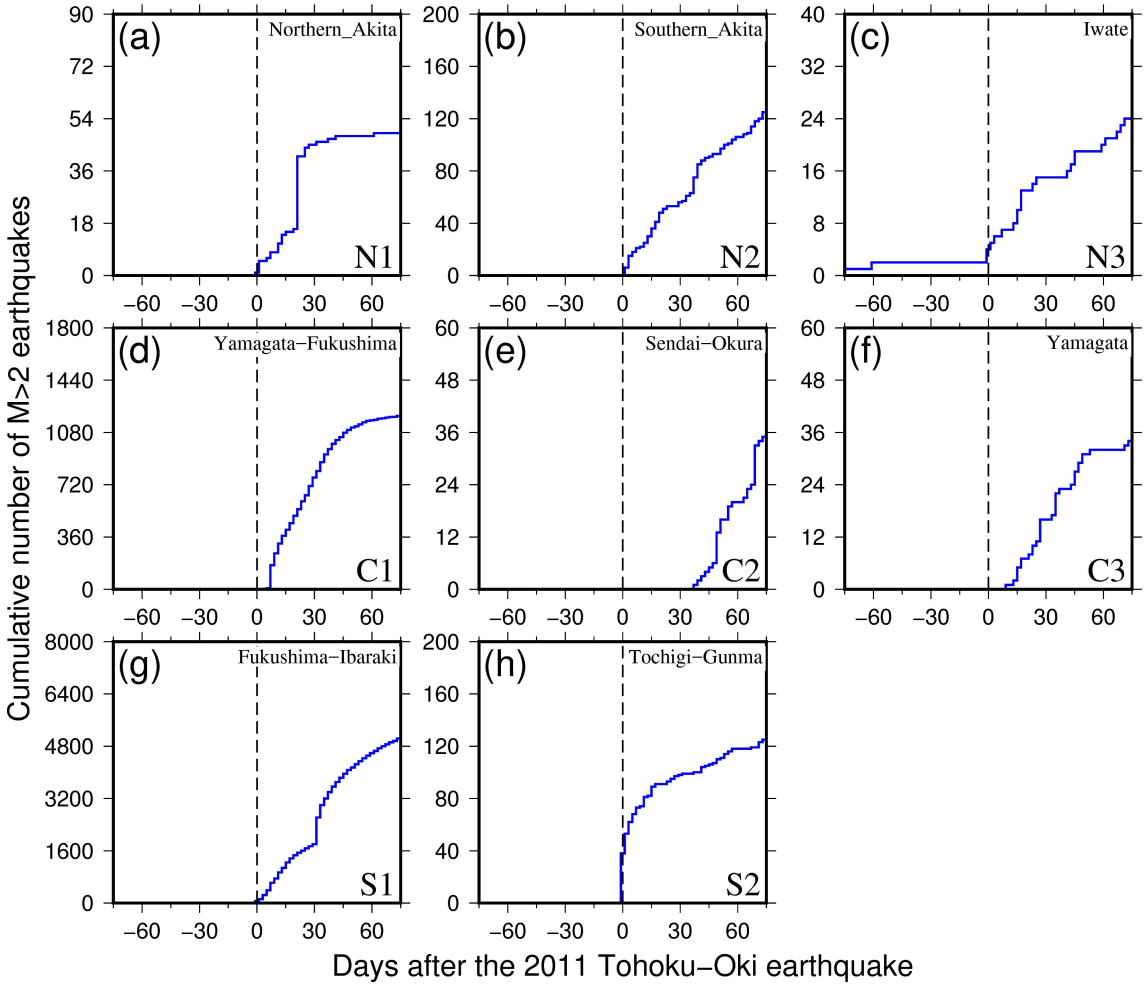
(a)
Northern_Akita
N1
(b)
Southern_Akita
N2
(c)
Iwate
N3
(d)
Yamagata−Fukushima
C1
(e)
Sendai−Okura
C2
(f)
Yamagata
C3
(g)
Fukushima−Ibaraki
S1
(h)
Tochigi−Gunma
S2
Cumulative number of M>2 earthquakes
Days after the 2011 Tohoku−Oki earthquake

Figure 3

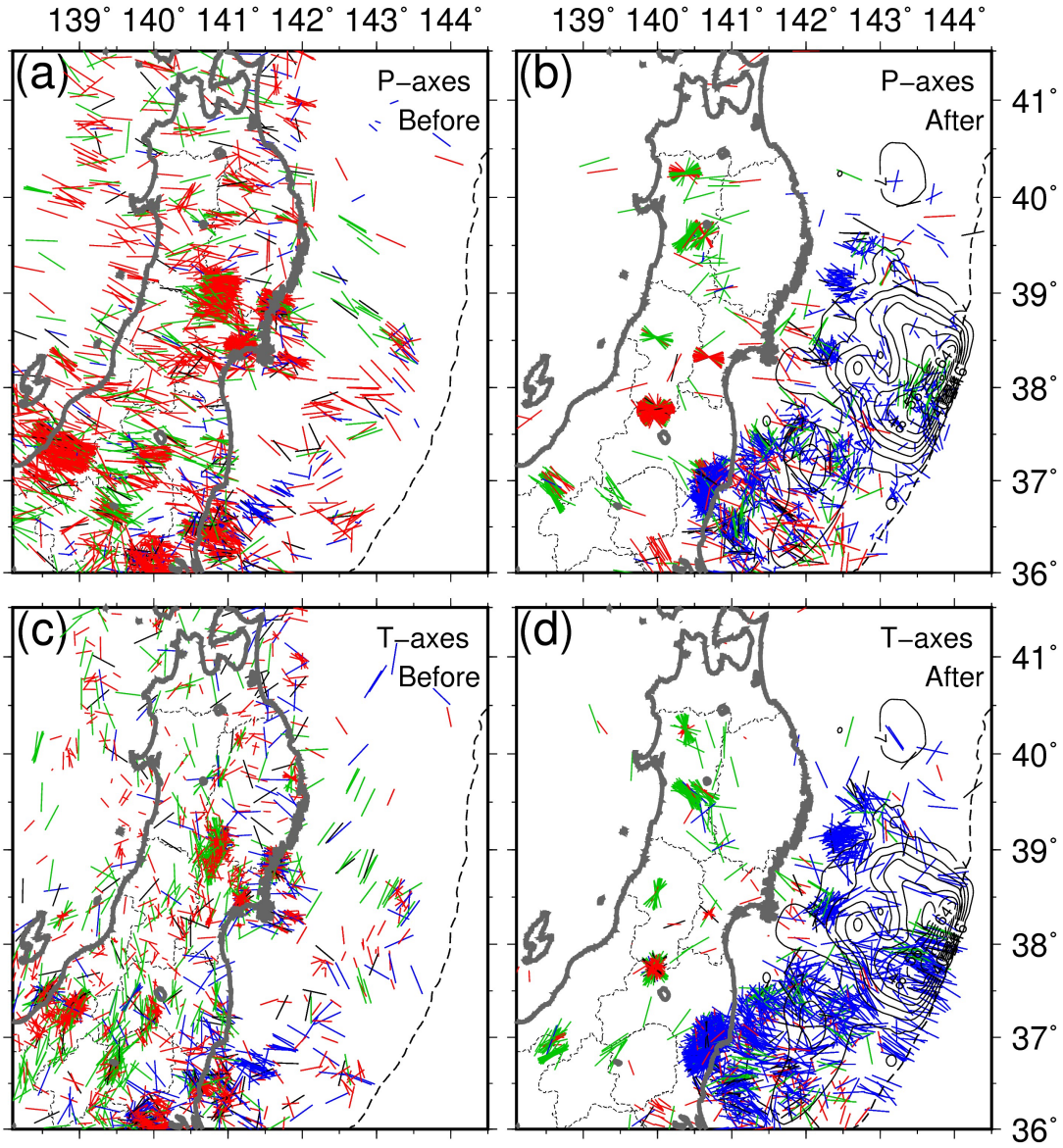
139° 140° 141° 142° 143° 144°
(a)
P−axes
Before
(b)
P−axes
After
(c)
T−axes
Before
(d)
T−axes
After
41°
40°
39°
38°
37°
36°

Figure 4

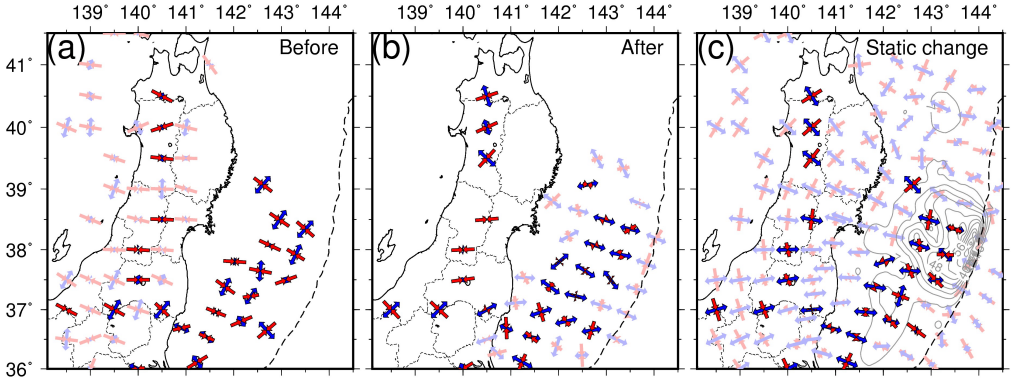
(a)
Before
(b)
After
(c)
Static change
139° 140° 141° 142° 143° 144°
41°
40°
39°
38°
37°
36°

Figure 5

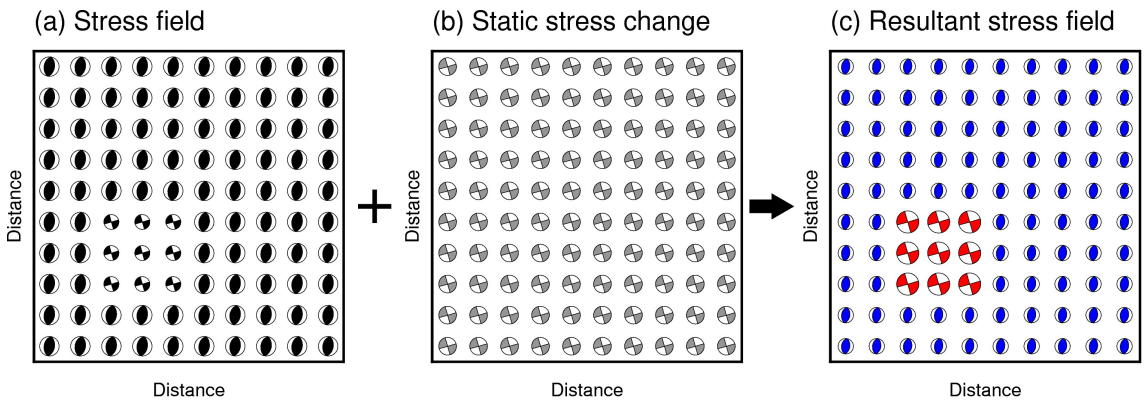
(a) Stress field
(b) Static stress change
(c) Resultant stress field
Distance
Distance
Distance
Distance
Distance
Distance

Figure 6

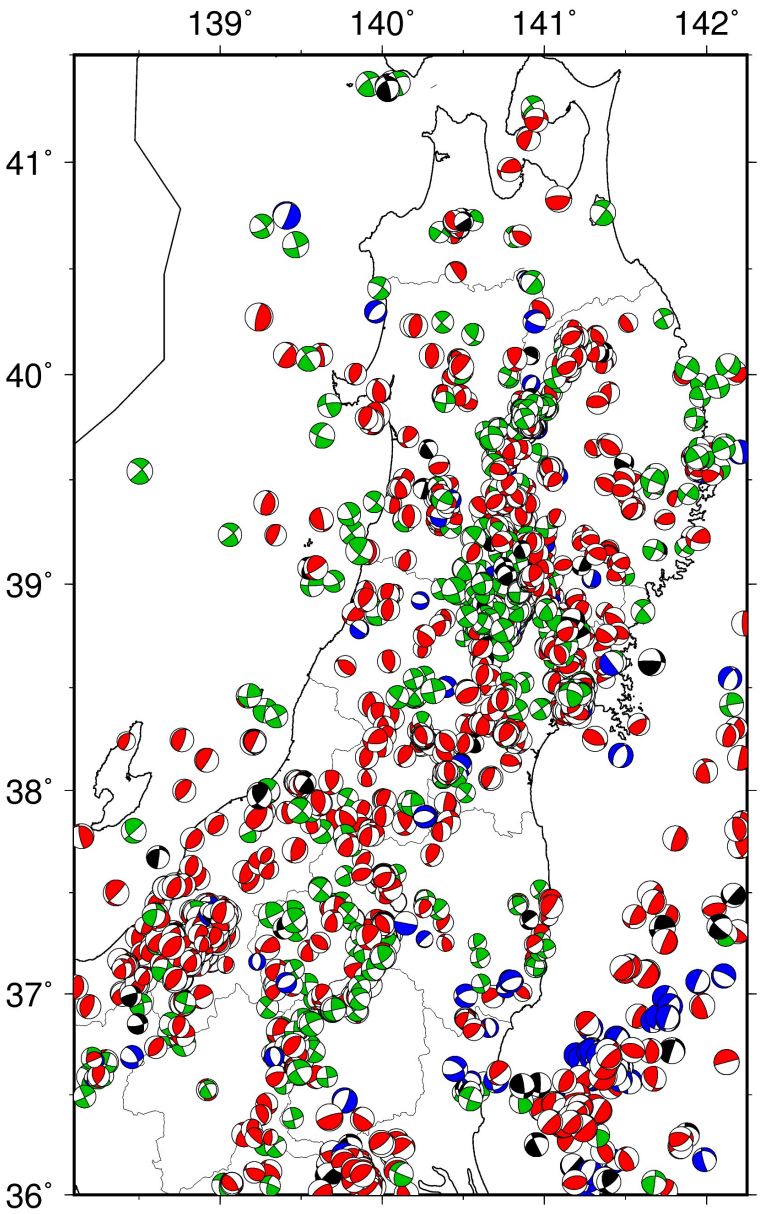

Figure 7

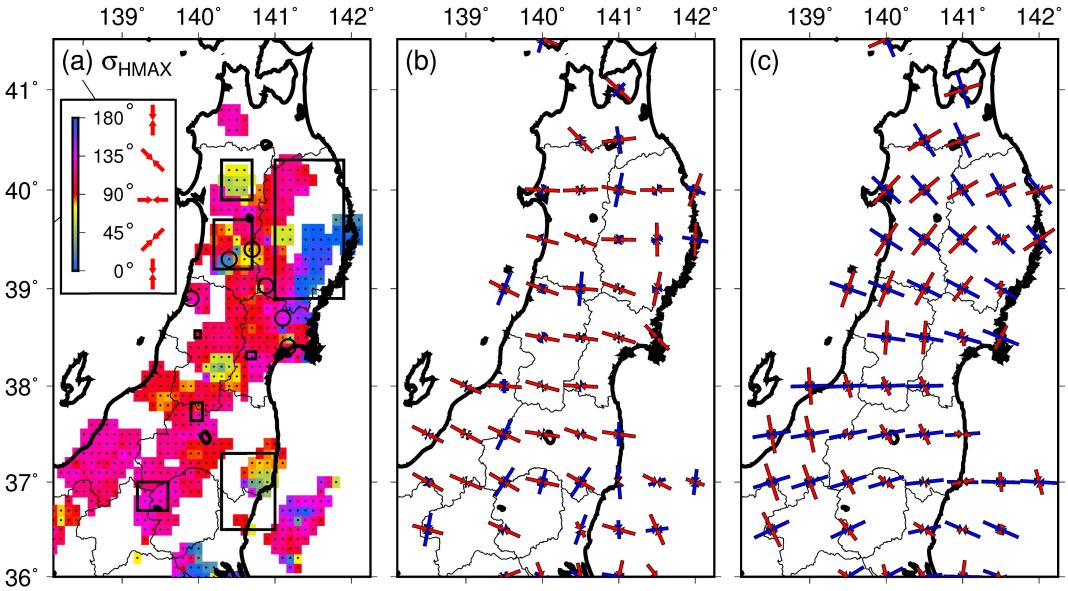

Figure 8

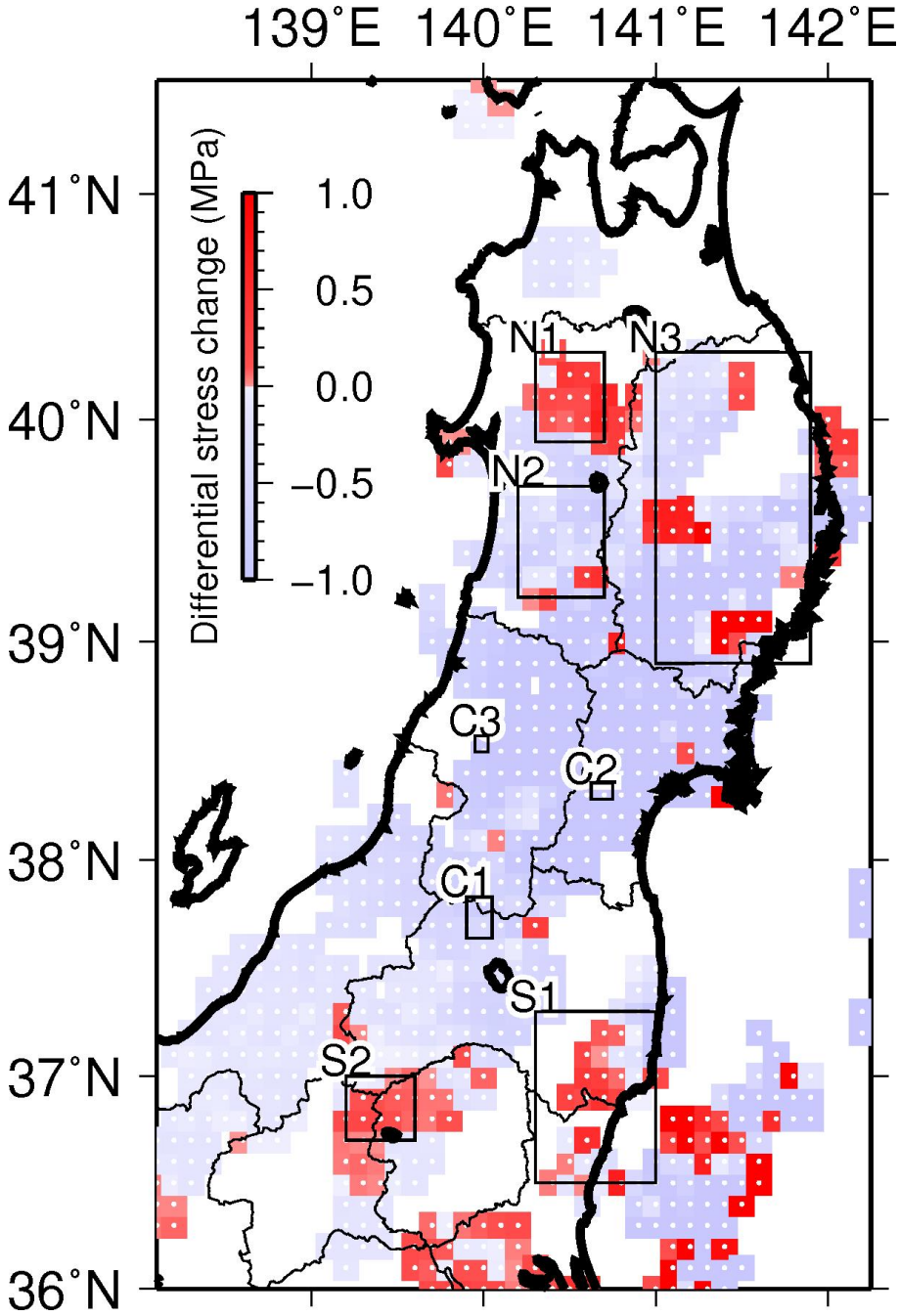
139˚E
140˚E
141˚E
142˚E
41˚N
40˚N
39˚N
38˚N
37˚N
36˚N
Differential stress change (MPa)
1.0
0.5
0.0
−0.5
−1.0
N1
N2
N3
C1
C2
C3
S1
S2

Figure 9

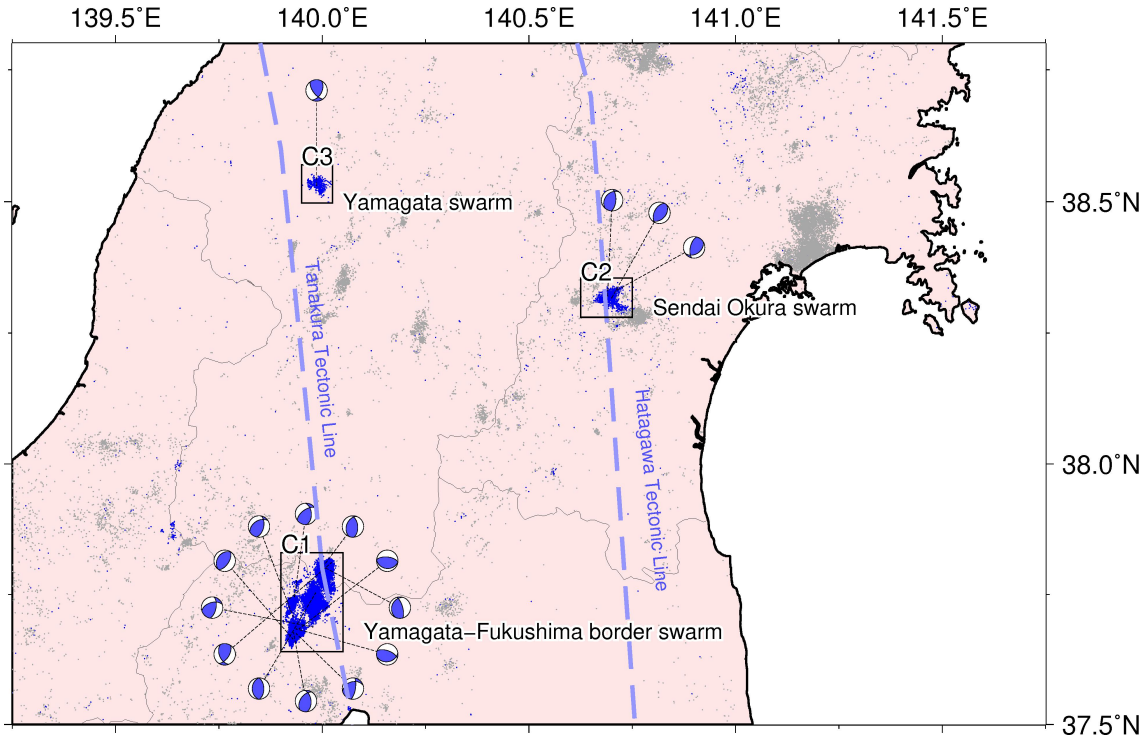
139.5˚E
140.0˚E
140.5˚E
141.0˚E
141.5˚E
38.5˚N
38.0˚N
37.5˚N
C3
Yamagata swarm
C2
Sendai Okura swarm
C1
Yamagata–Fukushima border swarm
Tanakura Tectonic Line
Hatagawa Tectonic Line

Figure 10

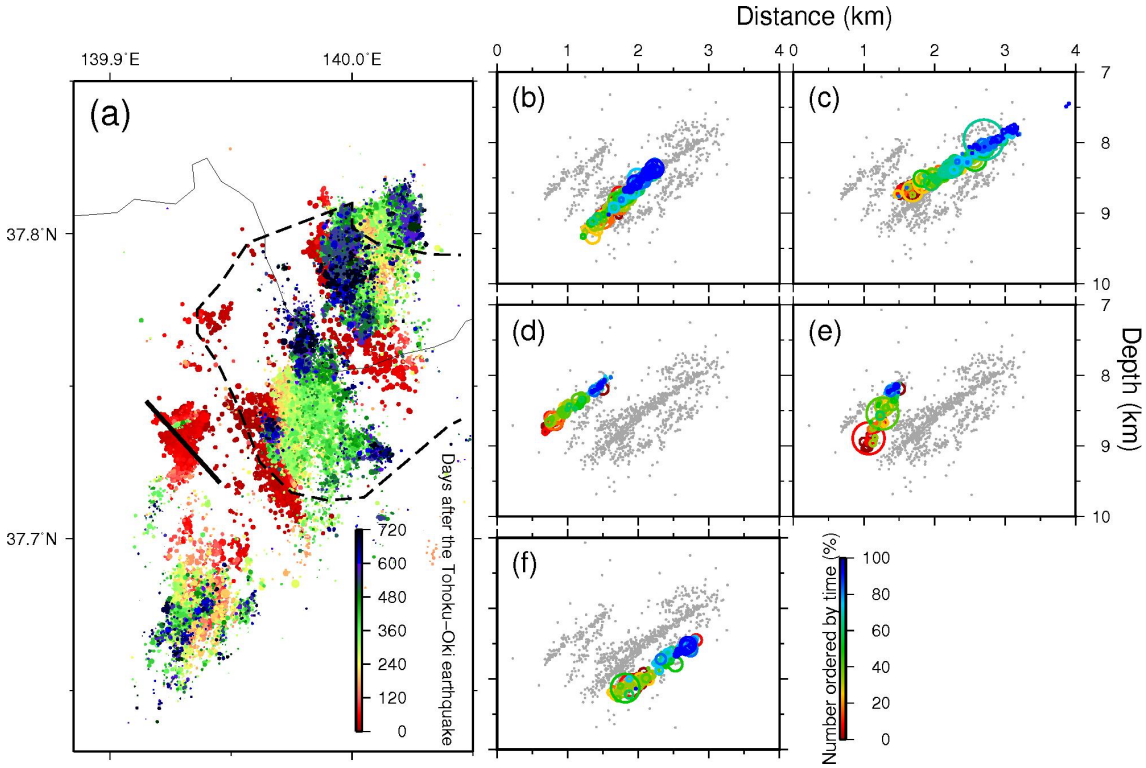
(a)
139.9°E
140.0°E
37.8°N
37.7°N
Days after the Tohoku−Oki earthquake
720
600
480
360
240
120
0
(b)
(c)
(d)
(e)
(f)
Distance (km)
Depth (km)
Number ordered by time (%)
100
80
60
40
20
0

Figure 11

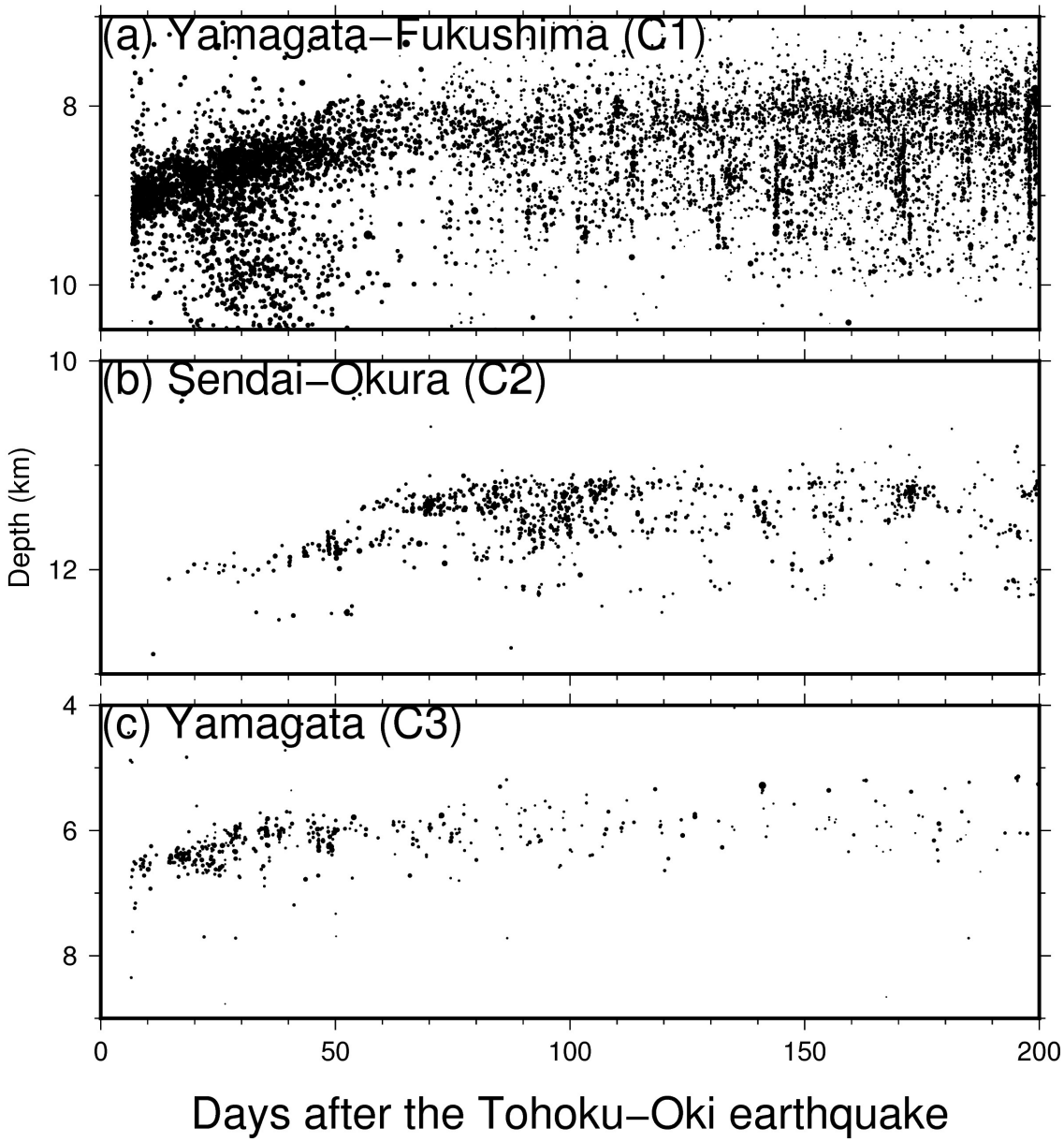
(a) Yamagata–Fukushima (C1)
8
10
(b) Sendai–Okura (C2)
10
12
Depth (km)
(c) Yamagata (C3)
4
6
8
0
50
100
150
200
Days after the Tohoku–Oki earthquake

Figure 12

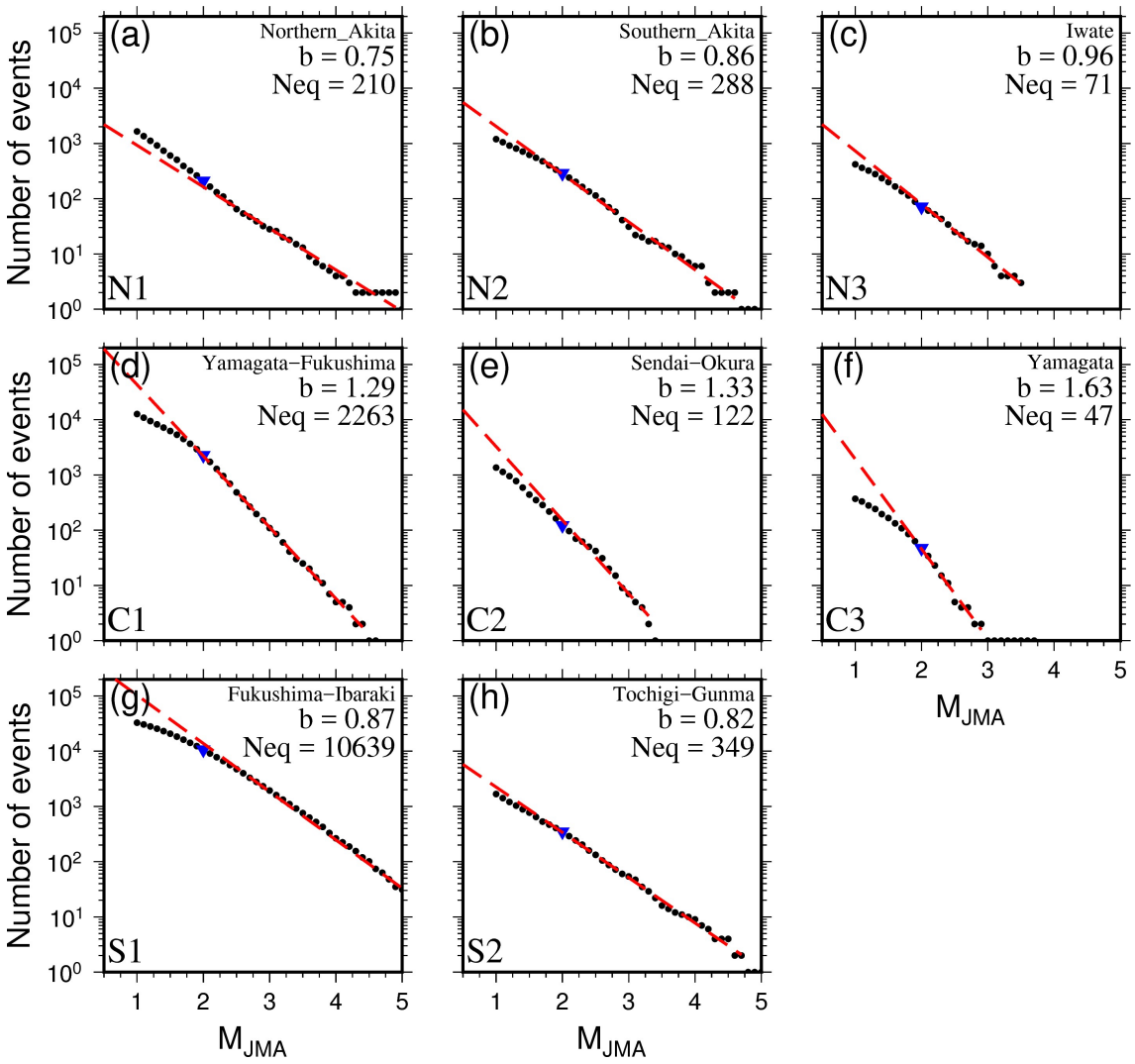
(a)
Northern_Akita
b = 0.75
Neq = 210
N1
(b)
Southern_Akita
b = 0.86
Neq = 288
N2
(c)
Iwate
b = 0.96
Neq = 71
N3
(d)
Yamagata−Fukushima
b = 1.29
Neq = 2263
C1
(e)
Sendai−Okura
b = 1.33
Neq = 122
C2
(f)
Yamagata
b = 1.63
Neq = 47
C3
(g)
Fukushima−Ibaraki
b = 0.87
Neq = 10639
S1
(h)
Tochigi−Gunma
b = 0.82
Neq = 349
S2
Number of events
M_JMA

Figure 13

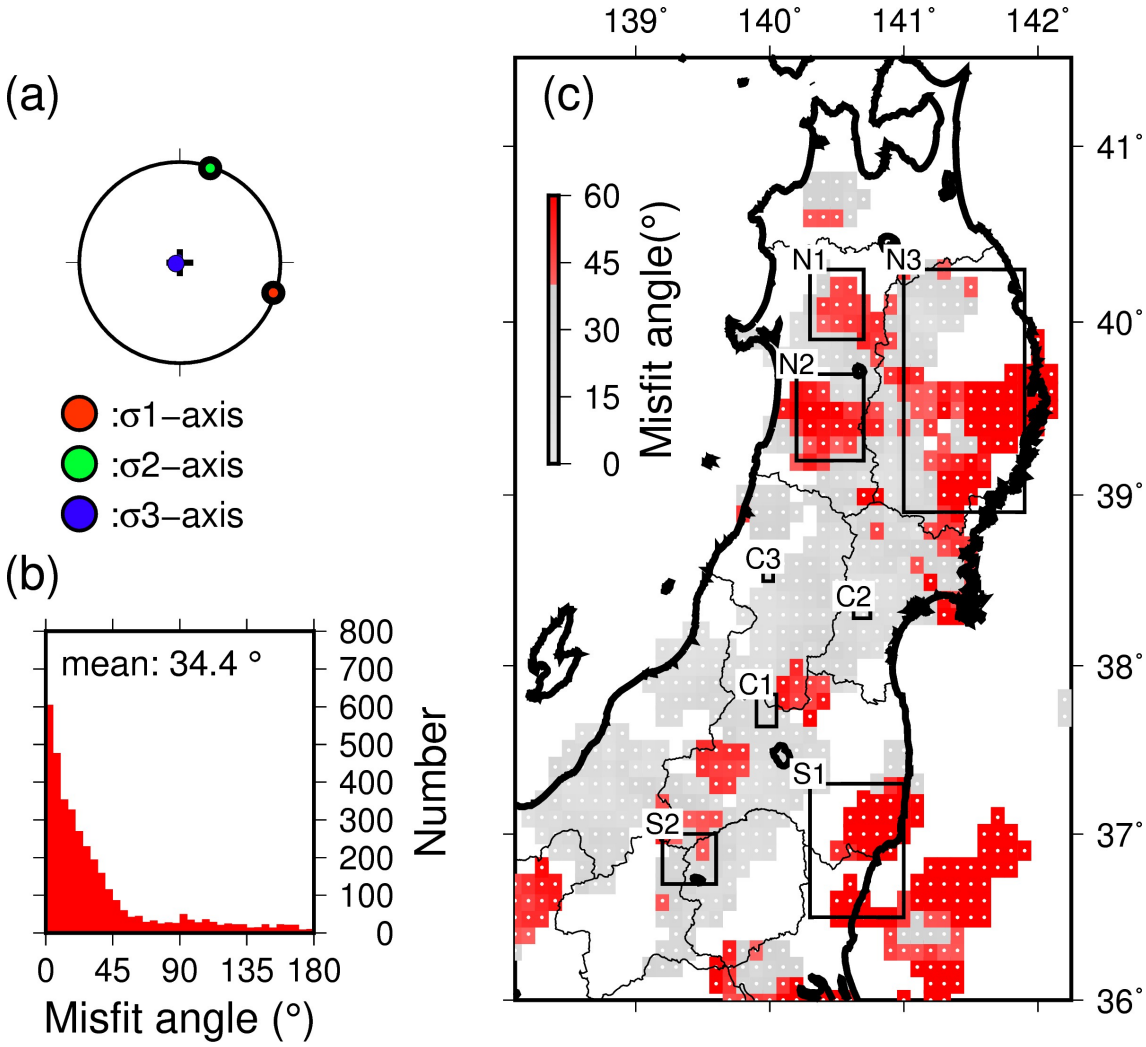
(a)
:σ1−axis
:σ2−axis
:σ3−axis
(b)
mean: 34.4 °
Number
Misfit angle (°)
0
45
90
135
180
800
700
600
500
400
300
200
100
0
(c)
Misfit angle(°)
60
45
30
15
0
139˚
140˚
141˚
142˚
41˚
40˚
39˚
38˚
37˚
36˚
N1
N2
N3
C1
C2
C3
S1
S2

Figure 14

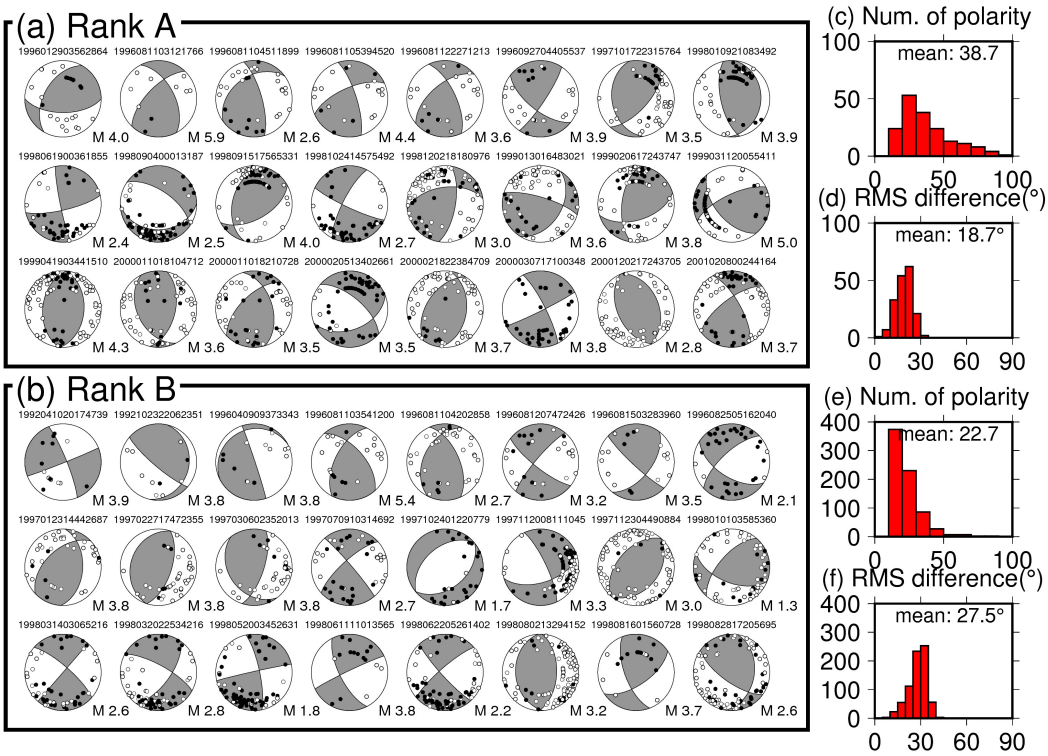
(a) Rank A
(b) Rank B
(c) Num. of polarity
mean: 38.7
(d) RMS difference(°)
mean: 18.7°
(e) Num. of polarity
mean: 22.7
(f) RMS difference(°)
mean: 27.5°

Figure S1